NAS 1.29/3-2:95-02

NASA Tech Briefs

National Aeronautics and
Space Administration

Electronic Components and Circuits

Electronic Systems

Physical Sciences

Materials

Computer Programs

Mechanics

Machinery

Fabrication Technology

Mathematics and Information Sciences

Life Sciences

95-02

COMPLETED

February 1995

INTRODUCTION

Tech Briefs are short announcements of new technology derived from the research and development activities of the National Aeronautics and Space Administration. These Briefs emphasize information considered likely to be transferable across industrial, regional, or disciplinary lines and are issued to encourage commercial application.

Availability of NASA Tech Briefs and TSP's

Distribution of NASA Tech Briefs, a monthly periodical publication, is limited to engineers in U.S. Industry and to other domestic technology transfer agents. Requests for individual Tech Briefs or for Technical Support Packages (TSP's) announced herein should be addressed to

NASA Center for AeroSpace Information
Technology Utilization Office
P.O. Box 8757
Baltimore, MD 21240
Telephone No. (301) 859-5300, Ext. 243, 245

Please reference the three-letter, five-digit control number located at the end of each Tech Brief. Information on NASA's Technology Utilization Program, its documents, and services is also available at the same facility.

Technology Utilization Officers and Patent Counsels are located at NASA field installations to provide technology-transfer access to industrial users. Inquiries can be made by writing to NASA field installations listed below.

Technology Utilization Officers and Patent Counsels

Ames Research Center
Technology Utilization Officer
Mail Code 223-3
Moffett Field, CA 94035

Patent Counsel
Mail Code 200-11
Moffett Field, CA 94035

Goddard Space Flight Center
Technology Utilization Officer
Mail Code 702-1
Greenbelt, MD 20771

Patent Counsel
Mail Code 204
Greenbelt, MD 20771

Lyndon B. Johnson Space Center
Technology Utilization Officer
Mail Code IC-4
Houston, TX 77058

Patent Counsel
Mail Code AL3
Houston, TX 77058

John F. Kennedy Space Center
Technology Utilization Officer
Mail Stop PT-PMO-A
Kennedy Space Center, FL 32899

Patent Counsel
Mail Code PT-PAT
Kennedy Space Center, FL 32899

Langley Research Center
Technology Utilization Officer
Mail Stop 143
Hampton, VA 23665

Patent Counsel
Mail Code 279
Hampton, VA 23665

Lewis Research Center
Technology Utilization Officer
Mail Stop 7-3
21000 Brookpark Road
Cleveland, OH 44135

Patent Counsel
Mail Code LE-LAW
21000 Brookpark Road
Cleveland, OH 44135

Jet Propulsion Laboratory
Technology Utilization Officer
Mail Stop 156-211
4800 Oak Grove Drive
Pasadena, CA 91109

NASA Resident Office-JPL
Technology Utilization Officer
Mail Stop 180-801
4800 Oak Grove Drive
Pasadena, CA 91109

Patent Counsel
Mail Code 180-801
4800 Oak Grove Drive
Pasadena, CA 91109

George C. Marshall Space Flight Center
Technology Utilization Officer
Code AT01
Marshall Space Flight Center,
AL 35812

Patent Counsel
Mail Code CC01
Marshall Space Flight Center,
AL 35812

John C. Stennis Space Center
Technology Utilization Officer
Code HA-30
Stennis Space Center, MS 39529

NASA Headquarters
Technology Utilization Officer
Code CU
Washington, DC 20546

Assistant General Counsel for Patent Matters
Code GP
Washington, DC 20546

Dryden Flight Research Center
Technology Utilization Officer
M/S D21-31
Bldg. 4832 Whse 7
Lilly Dr.
Edwards, CA 93523

BLANK PAGE

NASA Tech Briefs
National Aeronautics and Space Administration

February 1995
95-02

4 Electronic Components and Circuits

10 Electronic Systems

18 Physical Sciences

26 Materials

30 Computer Programs

32 Mechanics

36 Machinery

42 Fabrication Technology

44 Mathematics and Information Sciences

48 Life Sciences

This document was prepared under the sponsorship of the National Aeronautics and Space Administration. Neither the United States Government nor any person acting on behalf of the United States Government assumes any liability resulting from the use of the information contained in this document, or warrants that such use will be free from privately owned rights.

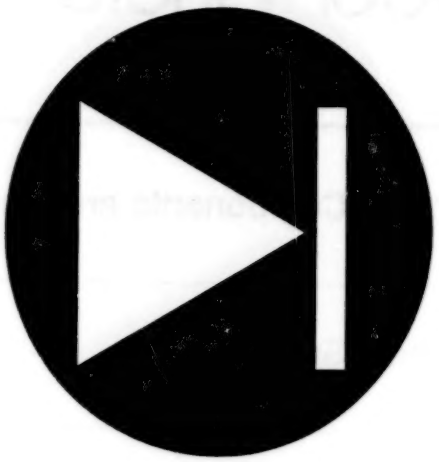

Electronic Components and Circuits

Hardware, Techniques, and Processes

5 Power MOSFETs Formed in Silicon Carbide
6 Flexible Multiplexed Surface Temperature Sensor
6 Rechargeable Magnesium Power Cells
7 Layout of Antennas and Cables in a Large Array
8 Measuring Work Functions of "Dirty" Surfaces With a Vibrating Capacitive Probe

4

Power MOSFETs Formed in Silicon Carbide

These devices could offer significant advantages over silicon-based devices.

Lewis Research Center, Cleveland, Ohio

High-performance power metal/oxide/semiconductor field-effect transistors (MOSFETs) have been fabricated in silicon carbide. These devices offer potential advantages over silicon-based MOSFETs, including lower "on"-state resistances at the same rated voltages, the ability to operate at higher temperatures (as high as 650 °C for some demonstration units), and higher thermal conductivity (with consequent ability to dissipate more power). SiC devices may also prove to be more resistant to damage by ionizing radiation — an advantage for switching applications in nuclear facilities.

The top part of Figure 1 illustrates the configuration of a vertically-oriented high-power SiC-based MOSFET with a UMOS structure made by use of trench-etching techniques and epitaxial growth to define the channel region. In the case of this n-channel device, an n^+ substrate is used for the drain contact. An n^- epitaxial layer of thickness and doping level required for the intended drain voltage of the FET is grown on the substrate. This n^- layer acts as the drain-drift region of the device.

A p-doped epitaxial layer is then grown, with a doping level and thickness chosen to prevent full depletion of the p layer when the intended drain voltage is applied to the p^+/n^- junction. The source wells can be formed either by implantation of n^+ ions into the p layer or by growing an n^+ epilayer on top of the p layer. In the latter case, it would be preferable to etch all the way through the central part of the n^+ layer so that the p layer makes contact with the source contact, as shown in the lower part of Figure 1. By thus short-circuiting the source and the p-doped channel layer together, one mutes the parasitic n/p/n bipolar transistor that is inherent in the structure.

The gate is formed by subsequently etching a trench through the n^+ well, p layer, and into the n^- drain-drift region. The gate oxide is then formed on the sides and bottom of the trench, and the gate contact is patterned onto the gate oxide. Thus, the inversion layer forms under the oxide on the side walls of the trench, between the n^+ source and the n^- drain, when a positive potential is applied to the gate contact. The etched sides of the trench can be sloped as in the figure, or vertical. Initial results have been achieved with these structures. The current-voltage characteristics of a small area SiC-UMOS MOSFET are shown in Figure 2. This device blocked 150 V and could achieve a drain current of 67 mA (100 A/cm^2) at a drain voltage of 3.3 V; This corresponds to a specific on-resistance of 33 mW-cm^2.

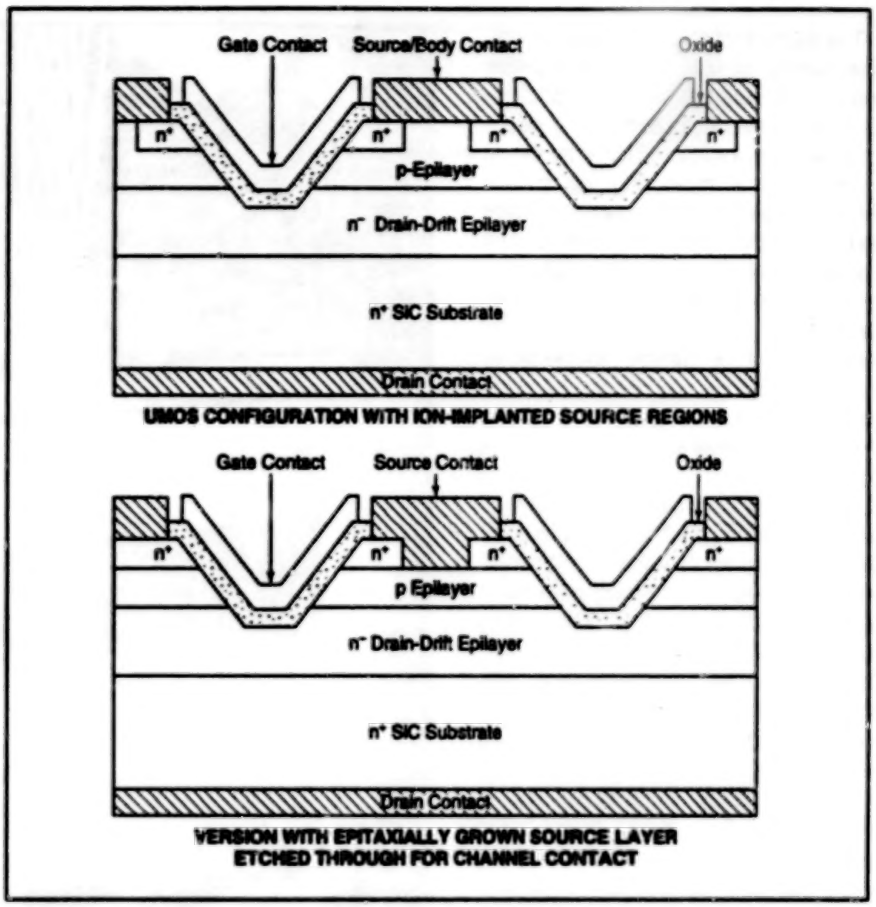

Figure 1. Power MOSFETs Can Be Formed in SiC in several alternative configurations. These are n-channel configurations.

This work was done by John W. Palmour of Cree Research, Inc., for **Lewis Research Center**. *Further information is contained in a TSP [see page 1].*

Title to this invention, covered by U.S. Patent No. 5,264,713 has been waived under the provisions of the National Aeronautics and Space Act (42 U.S.C. 2457 (f)). Inquiries concerning licenses for its commercial development should be addressed to

Cree Research, Inc.
2810 Meridian Parkway
Durham, NC 27713

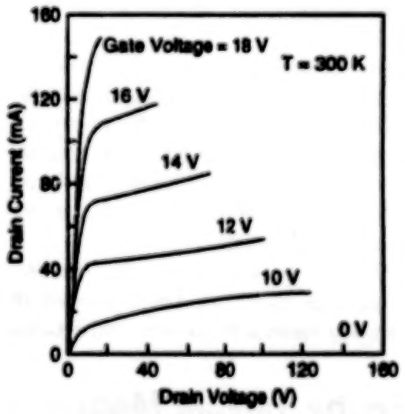

Figure 2. These Curves Show the Electrical Characteristics of a 150-V 4h-SiC vertical UMOS MOSFET. The area of this MOSFET is 6.7 x 10^{-4} cm^2.

Refer to LEW-15350, volume and number of this NASA Tech Briefs *issue, and the page number.*

BEST COPY AVAILABLE

Flexible Multiplexed Surface Temperature Sensor

Multiplexing enables rapid scanning of temperatures on aerodynamic surfaces.

Langley Research Center, Hampton, Virginia

The figure illustrates a surface temperature sensor or, more precisely, a unitary array of sensors that measure temperatures at points distributed over a designated area on a surface. The array should prove useful in measuring the surface temperatures of aerodynamic models and thermally controlled objects. The measurement of surface temperatures is important for designers and researchers. Heretofore, most approaches to the measurement of surface temperatures have involved the attachment of many single sensors to the surfaces of interest. The unitary array of sensors represents a novel approach.

The unitary array measures 1 by 4 in. (about 2.5 by 10 cm). It is made of a combination of integrated-circuit microchips and film circuitry. The circuitry consists of gold conductors etched on flexible polyimide film 0.002 in. (≈0.05 mm) thick. Eight AD590 temperature-sensing integrated-circuit microchips are mounted on the film: Eight sensor channels were selected to demonstrate the concept, but in principle, larger arrays (128, 512, or more temperature-sensing chips) could be constructed. The temperature-sensing chips can be scanned (that is to say, polled) at speeds approaching 10 kHz by use of a CD4051B analog multiplexing chip. The operating range of the sensor is –40 °C to 120 °C with a digital output that varies linearly with temperature at a rate of 1 μA/°C.

The flexibility of the array enables it to conform to curved surfaces. The multiplexer eliminates the need for numerous monitoring cables. Control of the acquisition and recording of data is effected by connecting the array to microcomputers via suitable interface circuitry.

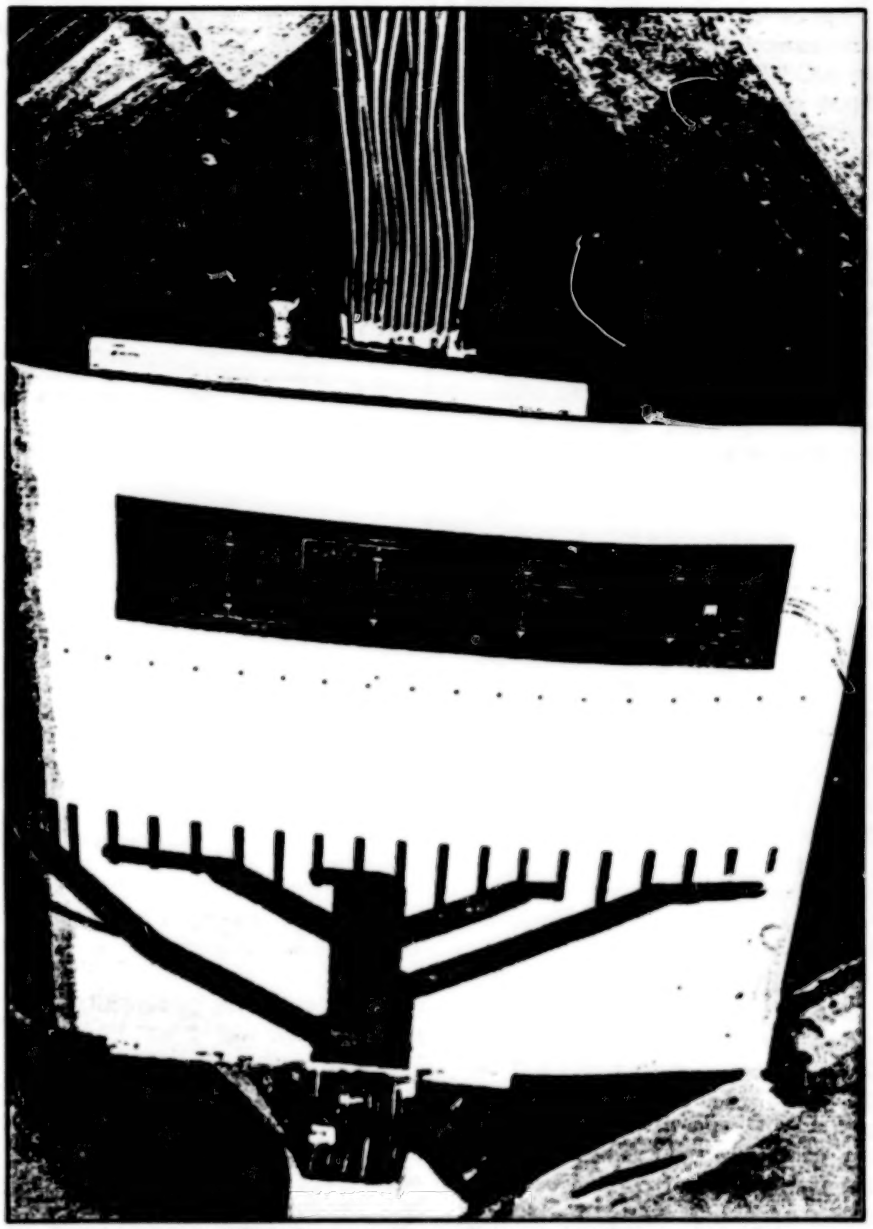

The Prototype Array of Eight Sensors with a multiplexer is installed on a test airfoil to measure surface temperatures.

This work was done by Kamran Daryabeigi and L. A. Dillon-Townes of **Langley Research Center** *and Preston B. Johnson and Robert L. Ash of Old Dominion University. Further information is contained in a TSP [see page 1].*

LAR-14003

Rechargeable Magnesium Power Cells

A moderate reduction in energy density would buy an increase in safety.

Lyndon B. Johnson Space Center, Houston, Texas

Rechargeable power cells based on magnesium anodes are being developed as safer alternatives to high-energy-density cells like those based on lithium and sodium anodes. Partly because of the low melting temperatures of lithium and sodium (179 °C and 98 °C, respectively) and partly because of the peculiarities of their electrochemistries, lithium- and sodium-based cells are both highly susceptible to catastrophic failures that release hot, toxic fumes and can cause fires.

Although the energy densities of magnesium cells are likely to be somewhat

BEST COPY AVAILABLE

6

smaller than those of lithium cells, magnesium offers important advantages: the melting temperature of magnesium is higher (651 °C), and magnesium compounds tend to exhibit low toxicity. Thus at the cost of some reduction in energy density, magnesium-based cells would be safer in that they would be much less susceptible to catastrophic meltdown followed by flames and venting of toxic fumes. Other advantages of magnesium include ease of handling, machining, and disposal, and relatively low cost of about $4.50/kg (1992 prices).

Magnesium cells containing an aqueous electrolyte have been used in military applications, but they are not rechargeable because of side reactions between the anodes and the electrolyte. Research on the feasibility of rechargeable magnesium cells has focused on two principal questions: (1) How do magnesium anodes behave in charge/discharge cycles in nonaqueous electrolytes? and (2) Are there high-voltage transition-metal oxide cathode materials into which Mg^{2+} can be inserted (similarly to the reversible insertion of Li^+ in CoO_2 and NiO_2)? The search has led to a prototype cell (see figure) composed of the following:

- An anode of magnesiated graphite ($Mg_x C_{12}$);
- An electrolyte consisting of 1 M $Mg(ClO_4)_2$ dissolved in a mixture of equal volumes of propylene carbonate (PC), ethylene carbonate (EC), and dimethyl carbonate (DMC);
- A ruthenium oxide cathode, which can participate in the 4-electron redox reaction $2\,Mg + RuO_2 \leftrightarrow Mg_2RuO_2$.

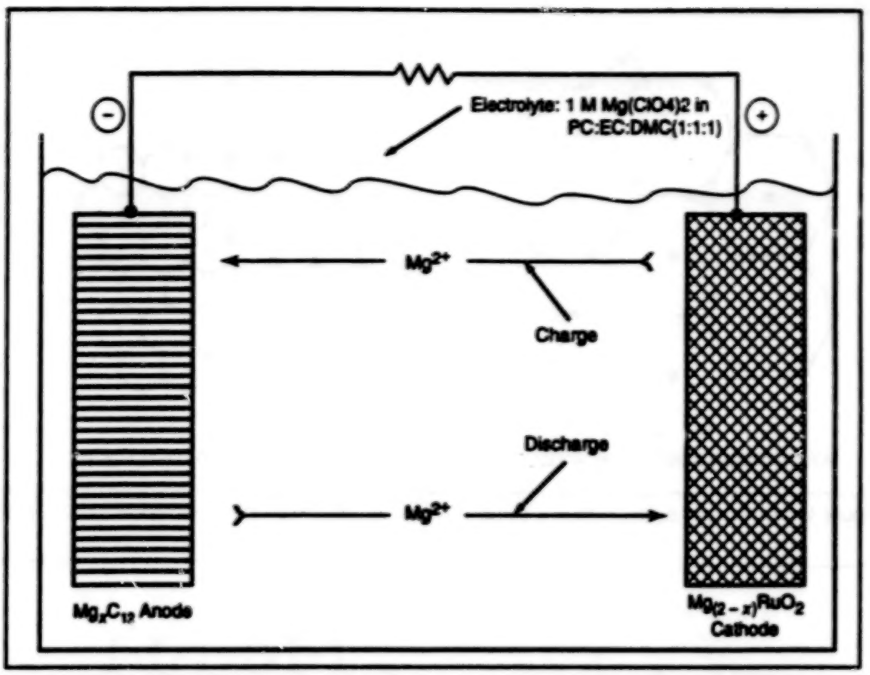

The Prototype Rechargeable Magnesium Cell operates according to a "rocking-chair" principle: Mg^{2+} ions from the electrolyte become alternately intercalated into the graphite anode (during charge) or the ruthenium oxide anode (during discharge).

The estimated practical energy density of a cell of this type constructed with typical hardware is 100 to 115 Wh/kg, which exceeds that of a typical nickel/cadmium cell (45 Wh/kg) or a nickel/metal hydride cell (75 Wh/kg). Preliminary experiments at 10 to 15 percent depth of discharge showed that cells of this type could be charged and discharged hundreds of times, albeit with some loss of capacity during the early cycles.

This work was done by Victor R. Koch, Chenniah Nanjundiah, and Michael Orsini of Covalent Associates, Inc., for **Johnson Space Center**. *Further information is contained in a TSP [see page 1].*
MSC-22293

Layout of Antennas and Cables in a Large Array

Total land area and the total length of cables are minimized.

NASA's Jet Propulsion Laboratory, Pasadena, California

A layout has been devised to minimize the total land area occupied by a large phased array of antennas and to minimize the total length of cables in the array. In the original intended application, the array would be an expanded version of the array of paraboloidal-dish microwave communication antennas of the Deep Space Network. The layout may also be advantageous for other phased arrays of antennas and antenna elements, including notably printed-circuit microwave antenna arrays.

In the original application, the minimum distance, L_{min}, between antennas is dictated by the requirement that an antenna not shadow an adjacent antenna down to a prescribed low angle of the line of sight above the horizon; in other applications like those mentioned above, L_{min} would typically be governed by mechanical or electromagnetic requirements. In either case, it is well known from mathematics and solid-state physics that the packing is densest (the total land area is minimized) when the antennas are arranged in a regular hexagonal pattern in which each antenna lies at the center of a regular hexagon circumscribed about a circle of diameter L_{min} and the hexagons are contiguous. The land area assigned to each antenna is $(3^{1/2}/2)L_{min}^2$ — the area of a circumscribed hexagon.

For maximum flexibility of operation, it is required that the array be divisible and subdivisible into smaller interlocking arrays that can be operated independently or in combinations. The hexagonal close packing must be maintained in any division or subdivision. It is required that each signal cable from each antenna be routed to a signal-processing facility at the center of the array. It is required to minimize the number of varieties of cables used throughout the array. No cable is allowed to cross another cable: in the original application, this prohibition is dictated by the requirement that cables be buried and by the consequent need to prevent snagging of previously buried cables by a cable plow. In other applications, (printed-circuit microwave antennas, for example), noncrossing of transmission lines could be dictated by

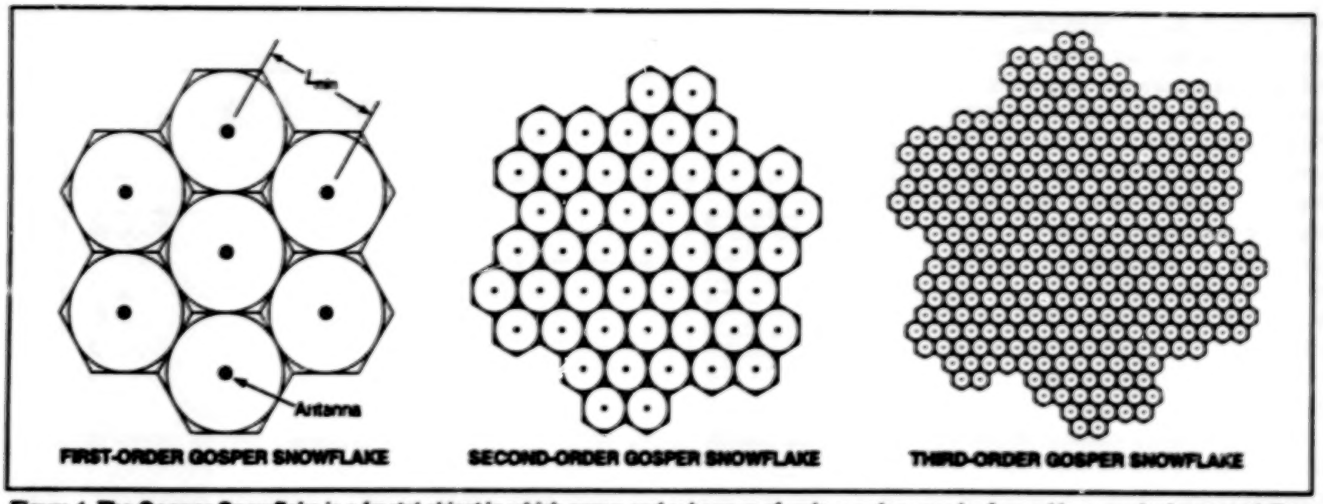

Figure 1. The **Gosper Snowflake** is a fractal object in which arrays and subarrays of various orders can be formed in a regular hexagonal tiling.

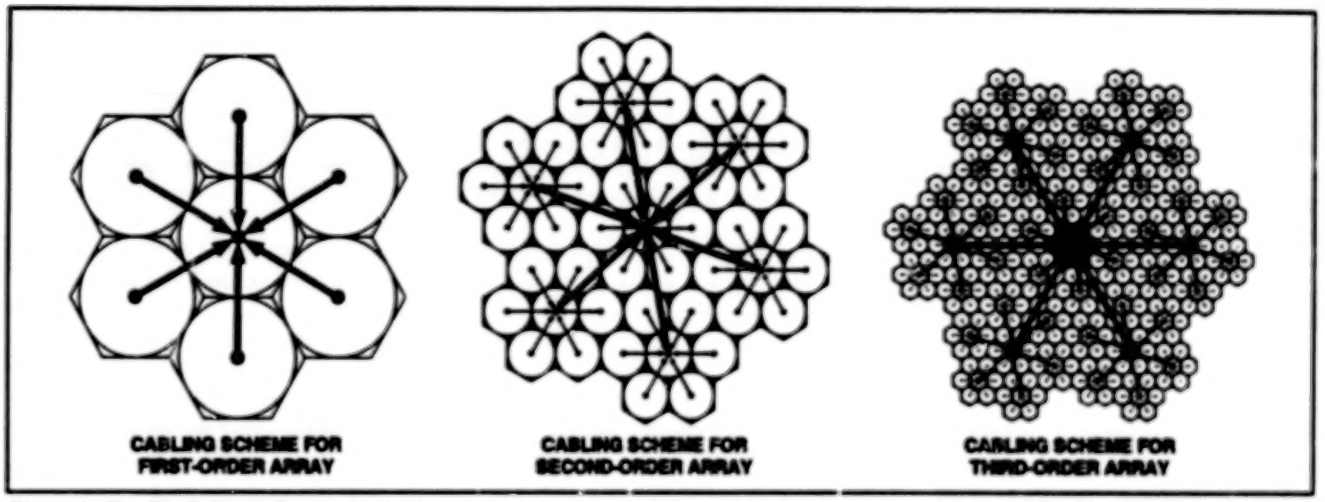

Figure 2. The **Six-Pointed Star** is the basic element of the noncrossing, minimum-total-length cabling scheme for antennas in a Gosper snowflake array.

the need to avoid the complexity and cost of multilayer circuitry.

The layout that satisfies these requirements while minimizing the total land area and the total length of cable is based on a fractal object known as the Gosper snowflake, which is formed from a recursive tiling of hexagons (see Figure 1). Starting with a single hexagon, the first-order Gosper snowflake is created by a first-order transformation in which each side of the hexagon is broken into segments of equal length, such that the original area of the hexagon is preserved. This first-order transformation is equivalent to grouping together of seven hexagons. The second-order Gosper snowflake is created in a second-order transformation, in which seven first-order Gosper snowflakes are grouped together. Similarly, and in general, a Gosper snowflake of order $N+1$ is created by grouping together seven Gosper snowflakes of order N.

The basic element of the minimum-length cabling scheme is a star that connects the six outer elements of the first-order Gosper snowflake to the central element. At the central element, the seven cables from the individual elements are spliced to a larger trunk cable. A similar structure of trunk cables connects the six outer first-order Gosper snowflakes to the center of the second-order Gosper snowflake to which they belong. In the same manner, larger trunk cables connect the six outer second-order Gosper snowflakes to the center of the third-order Gosper snowflake to which they belong. This scheme can be carried to higher orders. However, at orders ≥4, the trunk cables that connect the third-order Gosper snowflakes to the center must be made crooked in some places to prevent crossing of cables.

This work was done by Ronald T. Logan, Jr., of Caltech for **NASA's Jet Propulsion Laboratory**. *Further information is contained in a TSP [see page 1].*
NPO-19264

Measuring Work Functions of "Dirty" Surfaces With a Vibrating Capacitive Probe

Variations in work functions are associated with variations in microstructure and with contamination.

Langley Research Center, Hampton, Virginia

An apparatus measures the work function (ϕ) of the possibly contaminated surface of a specimen of metal or other electrically conductive material. The apparatus is designed for use in conjunction with improved photoelectric

and other techniques for measuring surface contamination; heretofore, the interpretation of photoelectric measurements has been complicated by the fact that both the intensity of photoemission of electrons (which is affected by ϕ) and ϕ itself can vary, not only with surface contamination, but also with the microstructure of the material to be inspected.

The apparatus, which is an application of the "Kelvin Probe" concept, measures the work function of the specimen in terms of the contact potential between (the difference between the work functions of) the specimen and a flat-plate probe that is made of a metal of known work function and is known to be clean. Despite the name "contact potential," the probe is not placed in direct contact with the specimen. Instead, the contact potential is measured with the associated circuitry shown in Figure 1.

The specimen is placed on a copper-clad surface that is mounted on an electrically insulating platform and maintained at a controllable dc bias voltage. The probe is positioned near and parallel to the surface of the specimen (see figure) and is vibrated, at a frequency of about 100 Hz, by use of a modified loudspeaker. The vibration gives rise to an oscillation between the flat-plate probe and the specimen, thereby generating an alternating voltage proportional to V, which equals the specimen/probe contact potential plus or minus, variously, the known bias voltage and the known contact potentials of intervening circuitry. This alternating voltage is buffered by a high-input-impedance operational amplifier and sent to a lock-in amplifier synchronized with the signal that drives the loudspeaker.

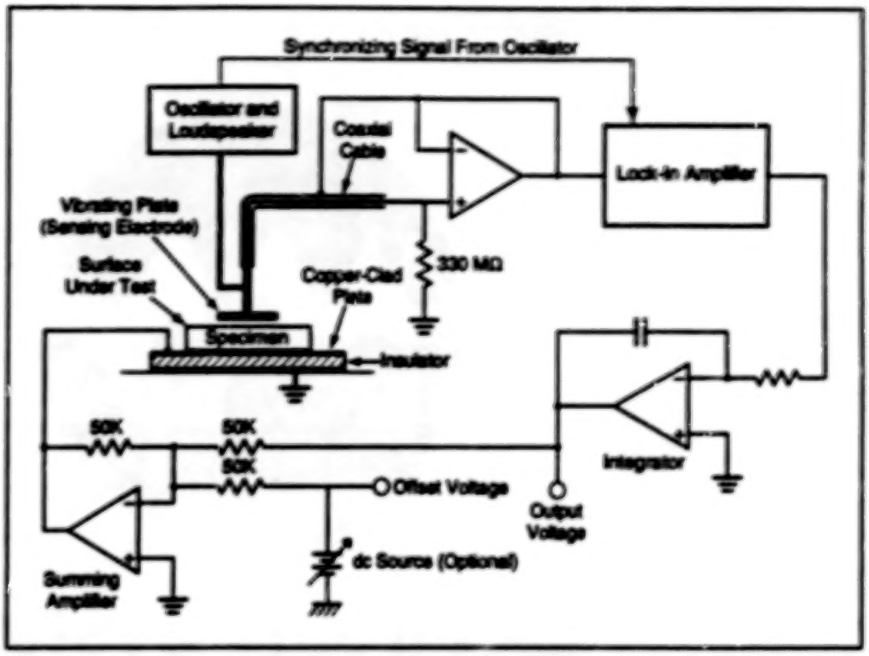

This Apparatus Measures the Work Function of the specimen indirectly, by vibrating capacitive measurement of contact potential. The work function of the specimen is affected by microstructure and by contamination.

The output of the lock-in amplifier is proportional to V. This output is fed to an integrator, the output of which is fed to one of the two input terminals of a summing amplifier to control the bias applied to the specimen. When the bias is such that V is zero, the output of the lock-in amplifier is zero and the output of the integrator stabilizes. At that point, the applied voltage is a measure of the contact potential between the specimen and the flat plate probe. An offset voltage can be fed to the other input terminal of the summing amplifier to test the circuit.

This work was done by William T. Yost of **Langley Research Center**. *No further documentation is available.*

Inquiries concerning rights for the commercial use of this invention should be addressed to the Patent Counsel, Langley Research Center [see page 1]. Refer to LAR-14671.

Electronic Systems

Hardware, Techniques, and Processes

11 Improved Noise-Power Estimators Based on Order Statistics
12 Improved Portable Ultrasonic Leak Detectors
13 Digital Control System for Wind-Tunnel Model
14 Phase-Locked Loop for Measurement of Small and Large Delays
15 Control Electronics for Reaction Wheel
15 Compensating for Apparent Strain at High Temperature
16 Wireless Headset Communication System
17 High-Density Digital Data Storage System

Improved Noise-Power Estimators Based on Order Statistics

Only one pass over the input data would be necessary.

NASA's Jet Propulsion Laboratory, Pasadena, California

A technique based on order statistics would enable the design of improved noise-power estimators. In the original intended application, the noise-power estimators would be part of the microwave-signal-processing system of the Search for Extraterrestrial Intelligence project. The improved technique is also applicable to other signal-detection systems and to image-detection systems that are required to exhibit constant false-alarm rates.

Order statistics are used because they provide noise-power estimates that are relatively insensitive to radio-frequency interference. Older noise-power-estimating techniques based on order statistics generally require multiple passes over the input data and thus tend to be too inefficient for real-time applications. The present technique involves limiting the dynamic range of the value to be estimated; this makes it possible to achieve the performance of an order-statistical estimator with simple algorithms and equipment and with only one pass over the input data.

In general, the computation of an order statistic of fixed rank requires sorting of the sample population, and sorting, in turn, requires multiple passes over the data. The advantages of the order-statistical approach (without the disadvantage of multiple passes over the data) can be obtained by fixing the value of the order statistic rather than fixing its rank, provided that the value remains within certain bounds. Accordingly, a new performance requirement called the "estimator dynamic range" is defined as the ratio between the largest and smallest values of the noise power (or other parameter) to be estimated, such that the estimator will perform within a specified error at all points between the two values.

One of the essential subsystems of a noise-power estimator according to the present concept is a threshold-and-count estimator (See Figure 1). This subsystem counts the members of a population of data that do not exceed a given threshold. Provided that the population is sufficiently dense around the threshold, the threshold-and-count operation is equivalent to choosing an order statistic for the noise-power estimate. However, the value of the order statistic and the threshold are fixed, and the rank of the order statistic is the random variable. The result is an estimate of the value of the cumulative distribution function at the threshold; that is, the probability that a datum lies below the threshold. The noise power can then be estimated from a lookup table, interpolating on the cumulative distribution function to recover the mean noise power of the population. A threshold-and-count estimator can be designed for a specified estimator dynamic range.

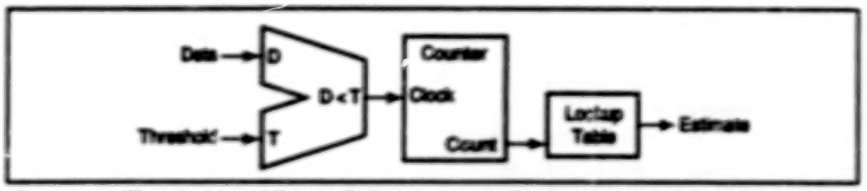

Figure 1. A Threshold-and-Count Estimator counts the data that are at or below a threshold value.

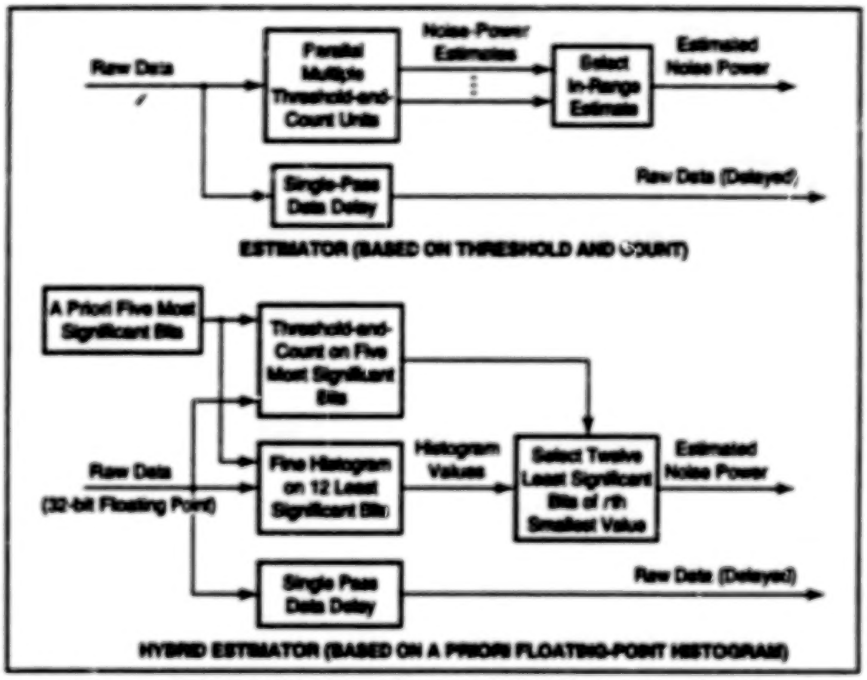
Raw Data
Parallel Multiple Threshold-and-Count Units
Noise-Power Estimates
Select In-Range Estimate
Estimated Noise Power
Single-Pass Data Delay
Raw Data (Delayed)
ESTIMATOR (BASED ON THRESHOLD AND COUNT)
A Priori Five Most Significant Bits
Threshold-and-Count on Five Most Significant Bits
Raw Data
(32-bit Floating Point)
Fine Histogram on 12 Least Significant Bits
Histogram Values
Select Twelve Least Significant Bits of rth Smallest Value
Estimated Noise Power
Single Pass Data Delay
Raw Data (Delayed)
HYBRID ESTIMATOR (BASED ON A PRIORI FLOATING-POINT HISTOGRAM)

Figure 2. These Proposed Noise-Power Estimators are based on the order-statistical concepts described in the text.

The top part of Figure 2 illustrates one noise-power estimator according to this concept: It would contain multiple threshold-and-count estimators that would operate in parallel on the same input data. The estimator dynamic ranges of these units would be made contiguous in the effort to ensure that there would always be one operating within its estimator dynamic range. The bottom part of Figure 2 shows an efficient single-pass hybrid estimator that would combine a threshold-and-count implementation with a histogram-based implementation. This estimator would be only slightly more complicated than the other one and considerably less complicated than a histogram-based true order-statistical estimator, yet would provide much greater dynamic range than is possible in a threshold-and-count-only implementation. The hybrid estimator would require only one threshold. It would produce an order statistic of desired rank, provided that the desired order statistic was within its dynamic range.

This work was done by George A. Zimmerman of Caltech for **NASA's Jet Propulsion Laboratory**. *Further information is contained in a TSP [see page 1].*

NPO-19213

Improved Portable Ultrasonic Leak Detectors

The primary advantage is greater sensitivity.

John F. Kennedy Space Center, Florida

Improved portable ultrasonic leak-detecting instruments have been designed to overcome some of the limitations of commercial instruments of this type. In the original application that motivated this development, a combination of high background noise in the testing environment and low sensitivity of the commercial leak detectors resulted in a tedious leak-detection process and marginal leak-detection performance. As compared with the commercial instruments, the improved leak detectors perform significantly better and are smaller and more rugged.

Ultrasonic leak detectors respond to jetlike leaks (leaks in which the flows are not laminar). The turbulence in a jetlike leak is accompanied by variations of pressure in the ultrasonic frequency range. Thus, an ultrasonic receiver with enough sensitivity and enough discrimination against background noise can be used to detect a small jetlike leak from a convenient distance.

The new instrument (see figure) includes an electronic module that processes the signal received from an ultrasonic-transducer module and feeds output to a set of headphones and/or to a multimeter. The ultrasonic-transducer module is connected to the electronic module via a cable that can be unplugged to connect another such module. Each ultrasonic-transducer module contains a commercial ultrasonic transducer of 40-kHz center frequency; this transducer features slightly more sensitivity and about half the noise of another 40-kHz commercial ultrasonic transducer that had been used in the commercial ultrasonic leak-detecting instrument that was replaced by the present instrument. The output of the ultrasonic transducer is preamplified before being transmitted through the cable to the electronic module.

Three interchangeable ultrasonic-transducer modules are supplied with each instrument. One of these modules is equipped with an ultrasound-collecting horn for use in scanning to detect leaks from a distance; the horn provides a directional sensitivity pattern with sensitivity multiplied by a factor of about 6 in the forward direction. Another module is similar except that it does not include the horn; this module is used for scanning close to a suspected leak, where the proximity of the leak more than offsets the loss of sensitivity occasioned by the lack of the horn. The third module is designed to be pressed against the leaking vessel; this module includes a rugged stainless-steel shell.

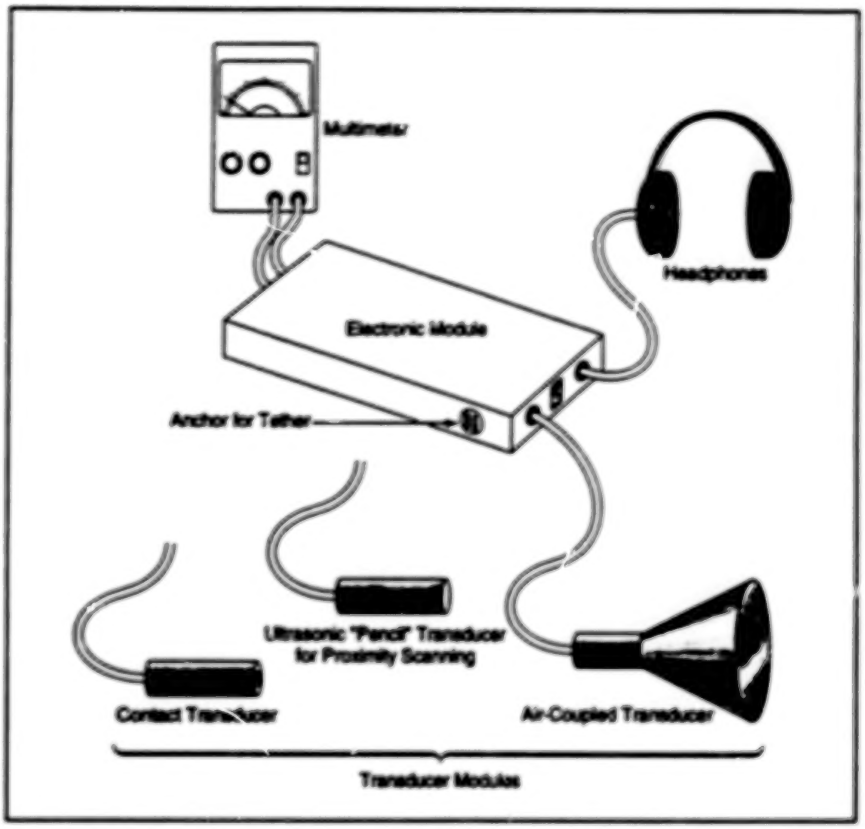

The Improved Portable Ultrasonic Leak Detector features three interchangeable ultrasonic-transducer modules, each suited for operation in a unique noncontact or contact mode.

In the electronic module, the preamplified output of the ultrasonic transducer is buffered, amplified further, then mixed with a 36-kHz signal from a local oscillator to shift the received ultrasonic signal to an audible frequency. The output of the mixer is low-pass filtered and amplified, yielding an audio signal containing frequencies of 2 to 6 kHz. The audio signal is sent to two optional output branches: in one branch, it is amplified for the headphones; in the other branch, it is amplified and half-wave rectified to provide a dc signal, proportional to the measured ultrasound, for the multimeter.

In practice, reading the multimeter appears to provide a slightly more sensitive indication of ultrasound than does listening via the headphones. The instrument is powered by two 9V batteries, which are contained in the electronic module. Tests have shown that the instrument can operate continually for more than 24 h on a pair of batteries. The estimated cost of a mass-produced commercial version of the improved ultrasonic leak detector with the horn transducer module should be less than $500 (based on prices of components in 1994). In contrast, the commercial ultrasonic leak detector that was replaced by this instrument costs more than $3,500.

This work was done by Robert C. Youngquist, John S. Moerk, William D. Haskell, Robert B. Cox, Jimmy D. Polk, James P. Strobel, and Frank Luaces of I-NET for **Kennedy Space Center.** *Further information is contained in a TSP [see page 1].*

Inquiries concerning rights for the commercial use of this invention should be addressed to the Patent Counsel, Kennedy Space Center [see page 1]. Refer to KSC-11751.

Digital Control System for Wind-Tunnel Model

Multiple functions are performed by multiple coordinated processors for real-time control.

Langley Research Center, Hampton, Virginia

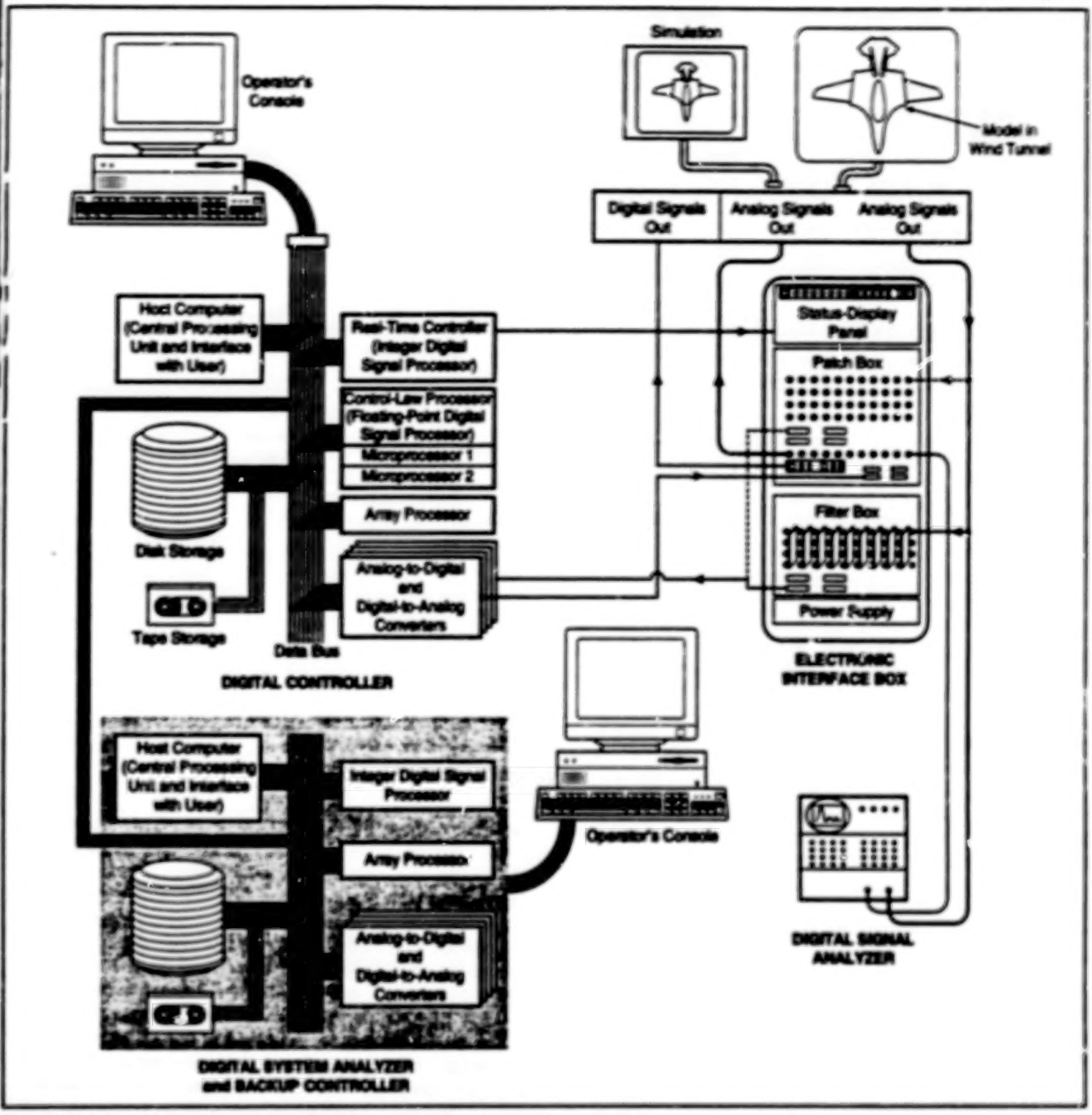

The Digital Control System provides flexibility in selection of control laws, sensors, and actuators, plus some redundancy to accommodate failures in some of its subsystems.

A multiple input, multiple-output, multiple-function digital control system has been developed for a wind-tunnel model of an advanced fighter airplane with actively controlled flexible wings. This control system interacts with sensors and actuators in the model, implementing a feedback control scheme that provides simultaneously for suppression of flutter, control of roll angle, roll-rate tracking during maximized roll maneuvers, and alleviation of loads during roll maneuvers.

The major subsystem of the digital control system is indicated by the box labeled "Digital Controller" in the figure. The digital controller includes a host computer (central processing unit) that serves as an interface with the user. The host computer is linked to several special-purpose processors via a data bus. One of the special-purpose processors is the real-time controller, which is an integer-arithmetic processor that operates at regulated speeds up to 200 Hz (in terms of time from sensor input to actuator-command output). This special-purpose processor synchronizes the operation of the other special-purpose processors and provides the user interface between the host computer and the real-time system.

it also coordinates the acquisition, transfer, and storage of data for real-time operation and for analysis of performance and estimation of parameters of the dynamics of the model and control system in nearly real time. The main reason for using the real-time controller (rather than the host computer) to synchronize and coordinate is that the host computer is too slow to effect real-time control: the operating-system software limits the speed of the host computer to about 60 Hz.

One of the other special-purpose processors is a floating-point digital signal processor containing two microprocessors that perform all the control-law computations. A third special processor is an array processor that performs floating-point calculations of flutter-suppression control laws in case the floating-point digital signal processor fails. The controller also includes circuits that perform all the necessary conversions between the digital forms of signals in the controller and the analog forms of signals in the sensors and actuators in the model. A second computer similar to the host computer is used to analyze the performance of the system in nearly real time and to estimate the parameters of the open- and closed-loop dynamics of the model and control system.

The design of the system provides flexibility in (1) the number, form, and functionality of control laws and (2) the selection of sensors and actuators used. In a demonstration, the system proved successful in suppressing flutter during various roll maneuvers. In particular, it provided active suppression of flutter in maneuvers that involved dynamic pressures up to 25 percent above the maximum allowable in open-loop control, both in cases in which the model was free to roll and in cases in which it was not free to roll.

This work was done by Sherwood T. Hoadley of **Langley Research Center** *and Sandra McGraw of Lockheed Engineering & Sciences Co. Further information is contained in a TSP [see page 1].*
LAR-14778

Phase-Locked Loop for Measurement of Small and Large Delays

Phase shifts from 0° to >360° can be measured to within 0.112°.

Langley Research Center, Hampton, Virginia

An electronic signal-generating and -processing subsystem of an ultrasonic inspection or measurement system consists mainly of a variable-and-fixed-frequency, pulsed phase-locked loop (VFFPPLL) that measures phase shifts from 0° to more than 360° with an accuracy of 0.112°. The VFFPPLL sends a toneburst to an ultrasonic transducer, which transmits the toneburst as a pulse of ultrasound into a specimen or acoustic-coupling medium. When the toneburst ends, the VFFPPLL and transducer go into a receiving mode: the echoes of the toneburst are received by the transducer, then amplified, then either (1) sampled directly or (2) mixed with a reference signal, then filtered, then sampled. The phase shift is then computed by comparing the phase of the sampled echo signal with that of the original toneburst. This phase shift is a measure of the ultrasonic-signal-propagation delay; it can be used, for example, to determine strain in a bolt or to track an irregular surface of a specimen that is being inspected ultrasonically.

The VFFPPLL (see figure) includes a personal computer that performs the control and digital signal-processing functions. Two numerically controlled oscillators (NCO1 and NCO2) driven by a common 50-MHz master clock generate tones at a common fixed or variable frequency ordered by the computer. The signal from NCO1 is the clock signal that governs sampling of the echo signal in the receivers; the signal from NCO2 is the tone that is gated to generate the toneburst in the transmitter. NCO1 and NCO2 operate at independently programmable phases.

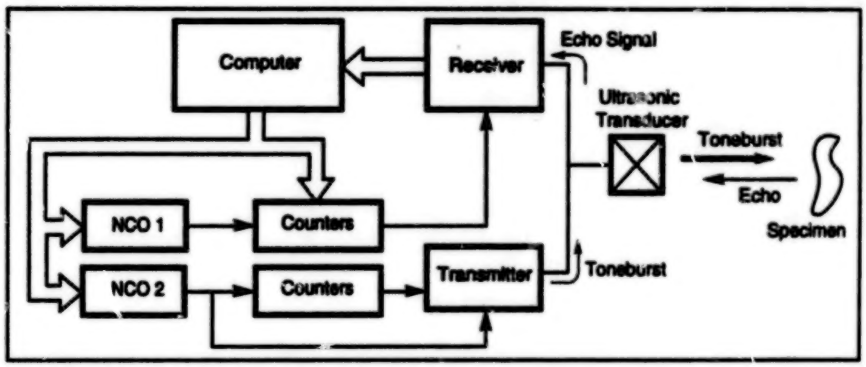

The VFFPPLL Measures the Phase Shifts between a transmitted ultrasonic toneburst and its echo, thereby measuring the ultrasonic-propagation delay.

Each box labeled "counters" in the figure denotes a 15-bit independently programmable divide-by-*N* counter and an 8-bit independently programmable downcounter triggered by the divide-by-*N* counter. The difference between the echo-signal-sampling time and the time of transmission of the toneburst is governed by the relative phases of the NCO1 and NCO2 signals that drive the divide-by-*N* counters, and equals the relative delay between the output pulses of the two pairs of counters. Acting via the 8-bit downcounters, the computer controls the durations of these pulses, thereby controlling the durations of the transmitted toneburst and the receiving pulse.

The receiving pulse can be used to drive a sample-and-hold circuit or to gate the input to an analog correlator. The output of the sample-and-hold circuit or analog correlator is fed to an analog-to-digital converter (ADC). The computer is programmed to accomplish phase lock by varying the frequency of the tone or the relative phases of the NCOs in such a way as to force the output of the ADC to zero. When phase lock is reached, the measured delay equals the difference between the phases (or the sum of incremental relative phase advances) of the NCOs divided by the angular frequency of the tone. The computer enables the use of sophisticated signal-processing and signal-recognition methods that enhance (in comparison with completely analog circuitry) the ability to find and hold phase lock.

This work was done by Mark Froggatt of **Langley Research Center.** *Further information is contained in a TSP [see page 1].*

Inquiries concerning rights for the commercial use of this invention should be addressed to the Patent Counsel, Langley Research Center [see page 1]. Refer to LAR-14840.

Control Electronics for Reaction Wheel

Bidirectional operation is achieved with a single-polarity main power supply.

Goddard Space Flight Center, Greenbelt, Maryland

The figure shows the major functional blocks of electronic circuitry that controls a two-phase ac induction motor with a reaction wheel attached to its shaft. The reaction wheel can store up to 0.8 ft-lb-s (about 1.1 J-s) of angular momentum at 250 r/min. The control circuitry is designed to supply pulse-width-modulated square drive waveforms, at 50 V peak to peak, to the two motor windings, 90° out of phase with each other, at an excitation frequency of 800 Hz.

The control circuitry operates partly in response to a digital magnitude-and-direction torque command generated by an external control subsystem and partly in response to tachometric feedback in the form of two once-per-revolution sinusoids with amplitudes proportional to speed. Operation can be in either of two modes called "normal" and "safehold." In the normal mode, the drive pulses are timed so that, on the average over one or a few cycles, the motor applies the commanded torque. In the safehold mode, the pulses are timed to keep the motor running at a set speed in one direction.

The control circuitry includes a pulse-width modulator (PWM) and a processor that computes a setting for the PWM on the basis of the actual speed and the most recently commanded torque. In the normal mode, torque commands are processed at a rate of 2 Hz. The digital output of the processor is converted to PWM-driving analog error signals. The PWM generates a four-phase, 800-Hz sequence of pulses. The durations of the pulses are controlled by the analog error signals via ramp-waveform voltage-to-time converter circuits.

The outputs of the PWM are fed, via optocouplers and other ancillary circuits, to eight metal oxide/semiconductor field-effect transistor (MOSFET) switches, which apply the drive pulses to the motor windings from a single +25-V power supply. The eight MOSFET switches are arranged in two four-switch H bridges — one H bridge for each motor winding. Each H bridge provides the required 50-V peak-to-peak square waveforms in the following way: During the first part of an 800-Hz cycle, one pair of MOSFET switches in the bridge is turned on to connect one side of the winding to +25 V and the other side to 0 V. During the second part of the cycle, the other pair of MOSFET switches is turned on to apply 25 V in opposite polarity. During intervals when all the MOSFET switches in a bridge are turned off, diodes direct flyback energy from the motor windings to the power supply.

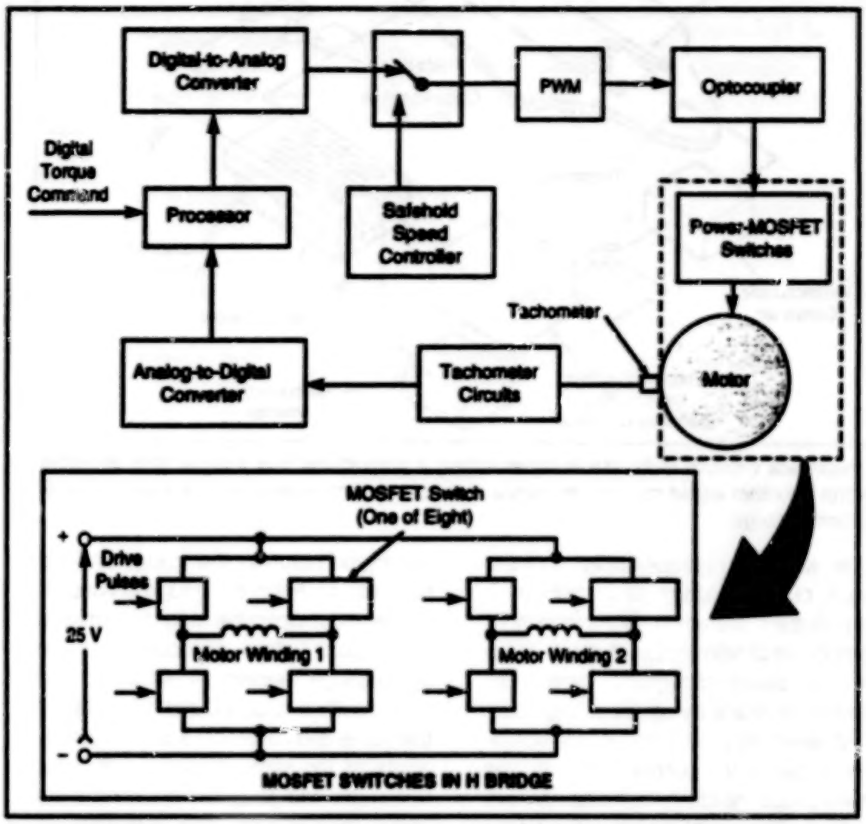

The Control Circuitry generates pulse-width-modulated 800-Hz waveforms to drive a two-phase ac motor and reaction wheel.

The control circuitry enters the safehold mode whenever an externally generated watchdog pulse has not been received within the past 5 seconds. In the safehold mode, the motor-drive pulses are applied or not applied in simple on/off fashion, depending on whether the speed is above or below a set value as indicated by comparison of the amplitude of the tachometer output with a set dc level: When the speed rises above the preset value, the motor drive is turned off and remains off until friction decelerates the motor and wheel below the preset speed.

This work was done by Keith Chamberlin of **Goddard Space Flight Center.** *Further information is contained in a TSP [see page 1].*
GSC-13593

Compensating for Apparent Strain at High Temperature

A control system would maintain a compensation strain gauge at the same temperature.

Langley Research Center, Hampton, Virginia

A proposed high-temperature strain-gauge system would include a subsystem that would compensate for apparent strain. There are many prior techniques for compensating for apparent strain, and each is more or less effective, depending on the specific application. The technique embodied in the proposed system is relatively complicated, but in return it offers the potential advantage of adaptability to a wide range of measurement conditions. In particular, the system should be able to

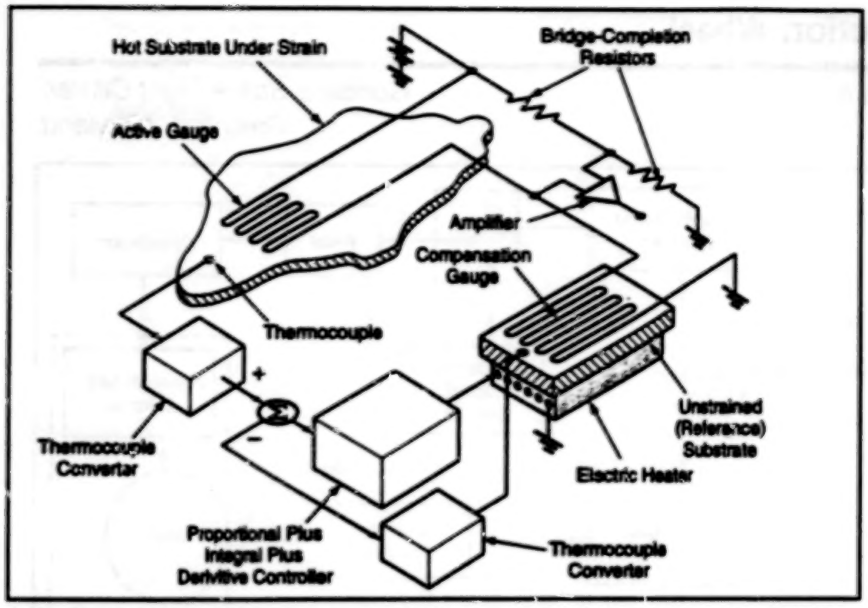

A Feedback Control Subsystem implementing a proportional plus integral plus derivative control algorithm would maintain the temperature of the compensation gauge equal to that of the active gauge.

cope with the nonrepeatable, nonlinear nature of the apparent-strain problem in complicated materials like matrix/fiber composites at high temperatures, at which apparent strains can greatly exceed real mechanical strains by orders of magnitude.

Apparent strain is a spurious temperature-dependent component of the strain-gauge reading, caused by two additive effects that occur in the strain-gauge installation. One effect is the variation of the electrical resistivity of the gauge material with temperature. The other effect is an apparent mechanical strain caused by differential thermal expansion between the gauge and the substrate to which the gauge is bonded.

The most desirable way to eliminate the apparent-strain component of the strain-gauge reading would be to use two matched gauges, each bonded in the same orientation on a separate substrate of the same material, with both substrates and gauges maintained at the same temperature. The substrate to which one of the strain gauges (the active gauge) was bonded would be the substrate undergoing the strain to be measured. The other substrate would remain unstrained, and the strain gauge bonded to this substrate would serve as a compensation gauge. Inasmuch as both gauges would be exposed to identical temperature and material environments, both would be subject to the same apparent strain. Thus, the gauge readings could be subtracted electrically in the Wheatstone bridge to obtain the true mechanical-strain component of the output of the active gauge.

Heretofore, it has been nearly impossible to implement this compensation scheme in practice because of various difficulties involved in keeping both gauges at the desired temperature under the required apparent-strain conditions. The proposed system would overcome the difficulties. The system (see figure) would include a thermocouple attached to the strained substrate, as close as possible to the active gauge. The compensation gauge and its substrate would be similarly instrumented with a thermocouple. The compensation gauge and substrate would be attached to a controllable electric heater. The Wheatstone-bridge-completion resistors would be housed in a signal-conditioning-and-power-supply electronic unit. A proportional plus integral plus derivative controller would continually adjust the power supplied to the heater, striving to keep the thermocouple outputs (and thus the temperatures of the substrates and strain gauges) equal.

This work was done by Harlan K. Holmes of **Langley Research Center.** *Further information is contained in a TSP [see page 1].*
LAR-14726

Wireless Headset Communication System

This system combines features of pagers, walkie-talkies, and cordless telephones.

John F. Kennedy Space Center, Florida

A wireless headset communication system uses digital modulation on a spread spectrum to avoid interference among units. The system consists of a base station, 4 radio/antenna modules, and as many as 16 remote units with headsets (see figure). The base station serves as network controller, an audio-mixing network, and an interface to such outside services as computers, telephone networks, and other base stations.

The remote units are battery-powered and weigh 18 oz (about 0.5 kg) each. The radio-frequency output power of each remote unit is 100 mW. A remote unit functions as a full telephone user interface via a keypad on the front cover. The user can set up conference calls, private calls, and ordinary telephone calls via simple keystroke sequences.

The radio/antenna modules communicate with the remote units via radio links in the frequency band from 902 to 928 MHz. The base station sends queries to the remote units sequentially; each headset is assigned a unique time slice in a time-division-multiplex protocol. A query is a data packet that contains a packet header, an address, some control information, and audio-signal data. A remote unit generates sound in the headset earphones according to the audio data. The packet contains enough data to produce the proper sounds until the next packet arrives. When a remote unit receives a query, the headset sends a response packet. Like a query packet, it contains a header, an address, control information, and audio data. The base station updates control settings according to the control information.

The radio/antenna modules can be as far as 1,000 ft (about 300 m) away from the base station. A remote unit can operate as far as about 500 ft (about 150 m) away from a radio/antenna module. Developed for use at Kennedy Space Center, the system could also be useful in industrial maintenance, emergency operations, construction, and airport operations. Also, its digital capabilities could be exploited; for example, by adding bar-code readers for use in taking inventories.

This work was done by Wilfred K. Lau, Richard Swanson, and Kurt K. Christensen of Telenexus, Inc., for **Kennedy Space Center.** *Further information is contained in a TSP [see page 1].*

In accordance with Public Law 96-517, the contractor has elected to retain title to this invention. Inquiries concerning rights for its commercial use should be addressed to

Wilfred K. Lau
1410 Summit Ave. Suite 1
Plano, TX 75074

Refer to KSC-11650, volume and number of this NASA Tech Briefs *issue, and the page number.*

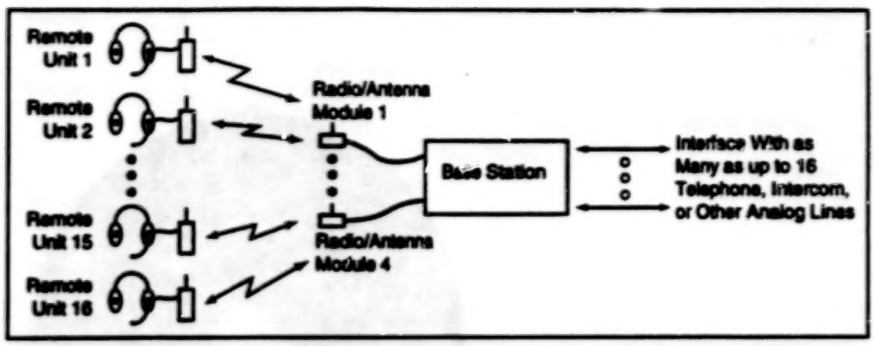
Remote Unit 1
Remote Unit 2
Remote Unit 15
Remote Unit 16
Radio/Antenna Module 1
Radio/Antenna Module 4
Base Station
Interface With as Many as up to 16 Telephone, Intercom, or Other Analog Lines

Workers Communicate With Each Other and with the outside world through portable headset units and a base station. Voice quality is good, with minimal echo.

High-Density Digital Data Storage System

This system stores 5 GB of digital data from a variety of sources.

Langley Research Center, Hampton, Virginia

A high-density digital data storage system is designed for cost-effective storage of large amounts of information acquired during experiments. (In the original application, the information consists of acoustic-measurement data.) The system can accept up to 20 channels of 16-bit digital data (see Figure 1) with overall transfer rates of 500 kilobytes per second. The data are recorded on 8-mm magnetic tape in cartridges, each capable of holding up to five gigabytes of data. Each cartridge is mounted on one of two tape drives. The operator can choose to use either or both of the drives. One drive can be used for primary storage of data while the other can be used to make a duplicate record of the data. Alternatively, the other drive can serve as a backup data-storage drive when the primary one fails.

The system includes data-input circuits, two microprocessors that operate the data-input circuits, small-computer-systems-interface (SCSI) tape-drive control units, and a control-and-display panel. An analog output for each channel is used to monitor the data signals sent to the tape drive(s) during recording or retrieved from the tape drive(s) during playback; two banks of digital-to-analog conversion circuits provide these analog outputs to the control-and-display panel. The system automatically searches for data on each tape that is loaded and enables front-panel controls either for a blank tape or a tape on which data are already recorded.

The operator can set the system to record data received on any number of input channels from 1 to 20. Incoming 16-bit serial data for each channel are fed to its data-input circuit (see Figure 2). In this circuit, the format of the data signal is converted from serial to parallel under the control of bit-clock and word-clock signals. Data in parallel format are then fed, in 8-bit units, to two first-in/first-out (FIFO) buffers that provide 2,048 samples of interim storage to compensate for any mismatch between the speed of input of data and the speed of recording of data on the tape. Address-logic circuitry provides addresses for encoding all 20 channels of input data onto a single tape channel and decodes the addresses to separate the data into their respective channels during playback.

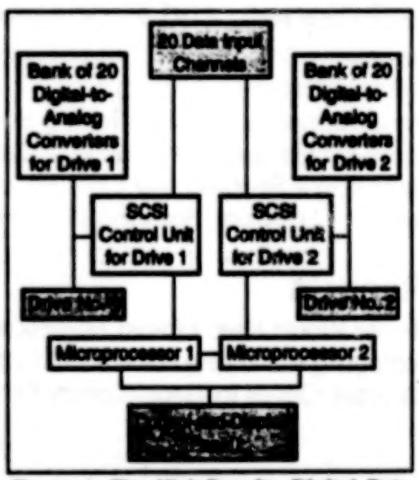
20 Data Input Channels
Bank of 20 Digital-to-Analog Converters for Drive 1
Bank of 20 Digital-to-Analog Converters for Drive 2
SCSI Control Unit for Drive 1
SCSI Control Unit for Drive 2
Drive No. 1
Drive No. 2
Microprocessor 1
Microprocessor 2

Figure 1. The High-Density Digital Data Storage System accepts data in as many as 20 channels of data, and records the data on one or two 8-mm tapes.

This work was done by Kenneth D. Wright and David L. Gray of **Langley Research Center.** *Further information is contained in a TSP [see page 1].*

This invention is owned by NASA, and a patent application has been filed. Inquiries concerning nonexclusive or exclusive license for its commercial development should be addressed to the Patent Counsel, Langley Research Center [see page 1]. Refer to LAR-14651.

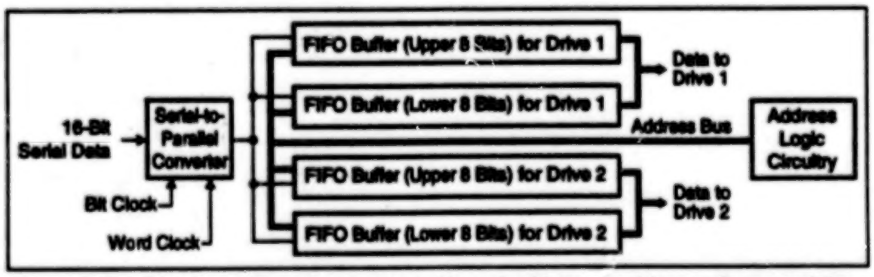
16-Bit Serial Data
Serial-to-Parallel Converter
Bit Clock
Word Clock
FIFO Buffer (Upper 8 Bits) for Drive 1
FIFO Buffer (Lower 8 Bits) for Drive 1
FIFO Buffer (Upper 8 Bits) for Drive 2
FIFO Buffer (Lower 8 Bits) for Drive 2
Data to Drive 1
Data to Drive 2
Address Bus
Address Logic Circuitry

Figure 2. The Data-Input Circuit associated with each of two tape drives performs serial-to-parallel conversion of incoming data and addresses and formats the data for recording.

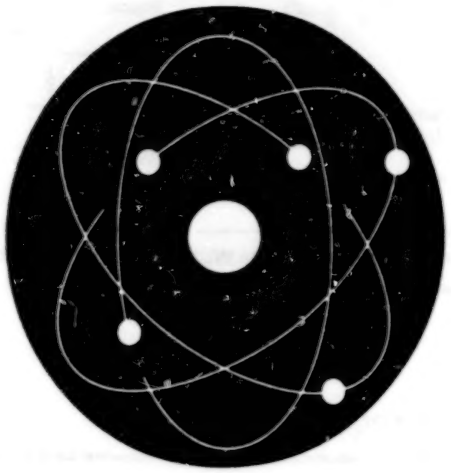

Physical Sciences

Hardware, Techniques, and Processes

19 Instruments Sniff Organic Surface Contaminants
20 Hydrogen-Detection Apparatus
21 Phase-Insensitive Ultrasonic Testing System
22 Apparatus Measures Permeation of Gases Through Coupons
22 Generating a Strobed Laser Light Sheet
23 Device for Ultrasonic Scanning of Curved Object

Books and Reports

24 Shades Would Keep Infrared Telescope Cold
24 Computing Microwave Force via Boltzmann-Ehrenfest Principle
25 Diffractive Optics for Geostationary Earth Observatory

Instruments Sniff Organic Surface Contaminants

Contaminants react with activated gas molecules, forming excited molecules that emit characteristic light.

John F. Kennedy Space Center, Florida

Portable instruments that detect both nonvolatile and volatile organic surface contaminants (principally, hydrocarbons) in real time are being developed. These instruments are easy to use: they operate under ordinary ambient atmospheric conditions, without need to use messy liquid solvents or to install and remove witness plates, and without need to cut specimens from the surfaces to be inspected. The principle of detection involves sweeping a pure, activated gas across the surface spot to be inspected, then monitoring light emitted at wavelengths characteristic of the excited molecules that are formed by chemical reactions between the activated gas and the contaminants.

The gas can be activated by a dc discharge, radio-frequency induction, microwave radiation, laser beam, hot filaments, or any other suitable means that excites some of the gas molecules. The preferred gas is nitrogen, the active species of which include single atoms of nitrogen and metastable, high-energy nitrogen molecules. One of the products formed in chemical reactions between organic materials and the active nitrogen species is excited cyanogen (CN), which emits light at a characteristic wavelength of about 385 nm.

The figure shows, schematically, one version of an instrument of this type. Here, the nitrogen gas is supplied as a regulated flow from a Dewar flask of boiling liquid nitrogen: it is advantageous to do this because at the temperature of liquid nitrogen, the vapor pressures of the hydrocarbon contaminants in commercially supplied nitrogen are much lower than the vapor pressure of the nitrogen, so that the nitrogen gas supplied is highly pure, as needed to prevent spurious contaminant readings.

The nitrogen gas is fed into a wand that is positioned on the surface spot to be inspected. The wand is essentially a specially designed gas-distributor head that directs the flow across the inspected surface. Spacer feet keep the wand at a fixed distance off the surface, thereby helping to ensure repeatability of readings. The slight positive pressure of the outflow of the nitrogen gas pushes ambient air out of the space between the wand and the inspected surface, so that the instrument does not read spurious atmospheric contaminants.

The nitrogen flowing into the wand is activated by a dc discharge between two electrodes. Fiber-optic cables are positioned to receive some of the light emitted by excited molecules entrained in the outflowing activated nitrogen gas. The fiber-optic cables are also aimed and positioned so as not to pick up light from the discharge and from short-lived excitation of residual contaminant molecules carried in from the nitrogen supply. The fiber-optic cables carry the light to bandpass filters, one of which passes the 385-nm light characteristic of cyanogen, the other of which passes the 380-nm light characteristic of nitrogen. The outputs of the filters are sensed by photodetectors, which thus give readings approximately proportional to the amount of contaminants and the amount of nitrogen, respectively. The cyanogen reading can be divided by the nitrogen reading to obtain a normalized contaminant reading that may fluctuate less with fluctuations in the degree of activation of nitrogen.

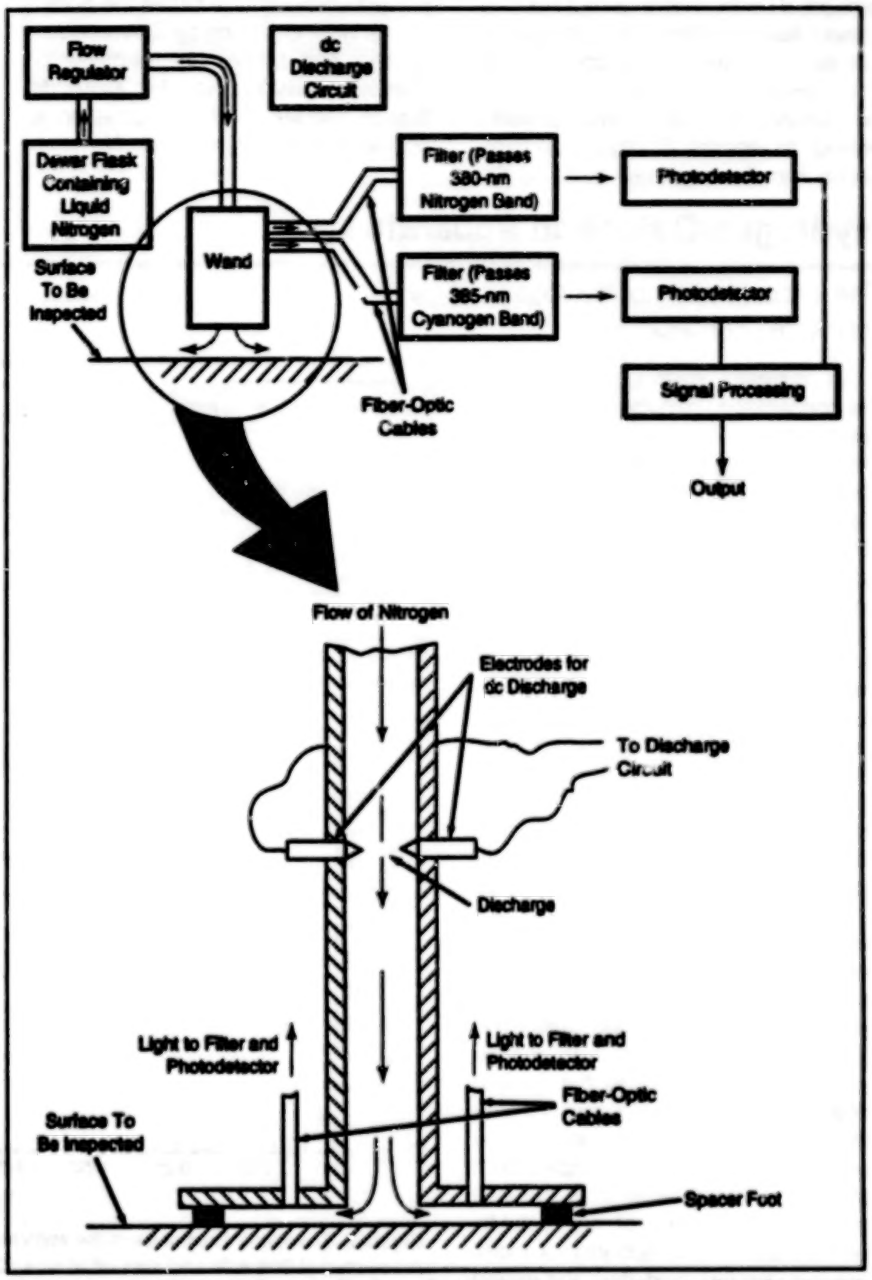

This Instrument Detects Organic Surface Contamination by applying a flow of activated nitrogen gas, then measuring light emitted by excited molecules formed in chemical reactions between the contaminants and the activated nitrogen.

The instrument as described thus far gives only a qualitative or semiquantitative indication of the amount of surface contamination. An alternative version (not shown in the figure) to measure the amount of contamination would include a pulsed laser and time-gated integrating circuits to process the outputs of the photodetectors. The laser pulse would be adjusted so that it was powerful enough to vaporize all organic contamination from the inspected spot, but not powerful enough to damage the spot. The time-gated, integrated 385-nm photodetector reading following a single laser pulse would thus be indicative of the total amount of contamination that was present on the surface before the pulse.

This work was done by Steven Adler-Golden and Michael W. Matthew of Spectral Sciences, Inc., for **Kennedy Space Center.** *Further information is contained in a TSP [see page 1].*

In accordance with Public Law 96-517, the contractor has elected to retain title to this invention. Inquiries concerning rights for its commercial use should be addressed to

Steven Adler-Golden
99 South Bedford St. No.7
Burlington, MA 01803-5169

Refer to KSC-11660, volume and number of this NASA Tech Briefs *issue, and the page number.*

Hydrogen-Detection Apparatus

The concentration of hydrogen can be monitored continuously.

Stennis Space Center, Mississippi

An apparatus continuously monitors the concentration of hydrogen, at a level ranging from a few parts per million to several percent, in a mixture of gases. Such a mixture could occur, for example, in a vessel that has been used to store or transport hydrogen and that has nominally been purged of hydrogen in preparation for maintenance or repair. The apparatus can be used to alert technicians to potentially explosive concentrations of residual hydrogen. In contrast, the older technique of collecting gas samples and taking them to an analytical laboratory for determination of the concentrations of hydrogen in them is time consuming and expensive and provides delayed measurements that are applicable only to the sampling instants.

In the apparatus (see Figure 1), the stream of gas to be sampled first passes through an oxygen-removing membrane, then toward a catalytic methanator. A feed stream of carbon dioxide gas is mixed with the sampled gas, and the resulting mixture is fed to the catalytic methanator. The catalyst in the methanator promotes the reaction between the hydrogen (if any) from the sample stream and the carbon dioxide from the feed stream. Downstream of the catalytic methanator, the concentration of methane is measured (and thus the relative concentration of hydrogen in the sampled gas is inferred) by use of a fixed-filter infrared detector.

The catalyst is designed for high methanation activity and minimal retention of product gases to achieve rapid response (see Figure 2). In fabricating a prototype of the catalyst, 0.65 weight percent ruthenium (as ruthenium chloride) was applied to low-specific-surface-area (0.4-m^2/g), 30-mesh-size alumina supporting particles with a pore size of 5.5 μm. About 1 g of the particulate catalytic material thus prepared was packed into a tube of 0.25-in. (6.35-mm) diameter. The resultant catalyst provides for a low metal support area with large pores and a high rate of conversion of CO_2 to CH_4.

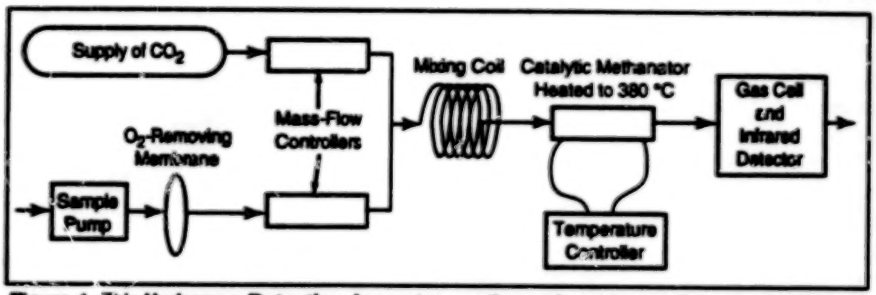

Figure 1. This Hydrogen-Detection Apparatus continuously measures the concentration of hydrogen in the sampled atmosphere.

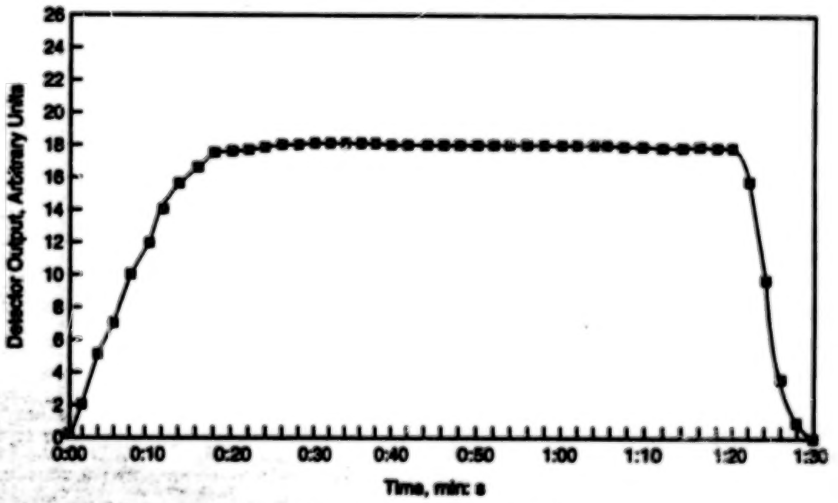

Figure 2. The Rapid Response of the apparatus is evident in this graph. The sample gas was introduced at time 0:00 and shut off at time 1:20.

The oxygen-removing membrane at the input end of the apparatus is necessary to provide an inert environment to the catalyst. The CO_2 feed stream and sample gas stream pass through mass-flow controllers, which provides a 1:1 mixing ratio. The catalytic methanator is heated to a temperature of 380 °C. The stream that leaves the catalytic methanator contains methane, oxygen, excess carbon dioxide, and other inert gas from the sampled atmosphere. The infrared detector that probes this stream is optimized for the detection of methane at a wavelength of 3.4 μm. It is simple and fast, providing high sensitivity and linear response.

This work was done by H. Richard Ross and Chris M. Bourgeois of Sverdrup Technology, Inc., for **Stennis Space Center.** *Further information is contained in a TSP [see page 1].*

Inquiries concerning rights for the commercial use of this invention should be addressed to the Patent Counsel, Stennis Space Center [see page 1]. Refer to SSC-00021.

Phase-Insensitive Ultrasonic Testing System

This system reveals disbonds at rough interfaces.

Langley Research Center, Hampton, Virginia

An ultrasonic testing system is being developed for use in revealing hidden disbonds at rough, inaccessible interfaces between layers of material. A rough surface or surfaces can introduce artifacts of two types into reflected ultrasonic signals. One type comprises severe artifacts of phase cancellation at the face of a typical phase-sensitive transducer used in conventional ultrasonics. The other type comprises artifacts caused by reflection of part or all of an ultrasonic beam away from a transducer. These artifacts can impair the detection of defects at interfaces. If an interface between two layers is rough and uneven, then it is difficult to detect disbonds between the layers by use of the pulse/echo technique.

If the excursions of a surface from flatness are of the order of a quarter of an ultrasonic wavelength or larger over lateral dimensions of the order of the width of the ultrasonic beam, then the ultrasonic signal can be severely compromised. Such is the case for the configuration of the bondline inhibitor, liner, and fuel at the ends of the segments of the solid rocket motor of the space shuttle. Here, the liner-to-fuel bondline is very rough with respect to the ultrasonic wavelength. The development of the present ultrasonic system and the phase-insensitive-array technique on which it is based was motivated by the need to detect disbonds under conditions like these.

The system includes an array of small (maximum dimension about a wavelength or less) piezoelectric transducers, the receiving outputs of which are electronically processed individually and combined in such a way as to make the system phase-insensitive, thereby overcoming the limitations imposed by the phase-sensitivity of conventional ultrasonic transducers. An array is technically feasible and offers the further advantage that the signals applied to elements of the array during transmission can be phase-controlled to focus the transmitted acoustic energy. A simple way to suppress the reflection-type artifacts is to use a receiving transducer that has a large area: by subtending a larger angle with respect to the apparent source of the signal in question, the receiving transducer receives more incident energy.

Thus, artifacts of both types could be suppressed by a phase-insensitive array of piezoelectric transducers that subtends a large angle. The array could then be used in a pulse mode like that of a conventional pulse/echo transducer during transmission, but during reception it would be phase-insensitive and less sensitive to reflection-type artifacts.

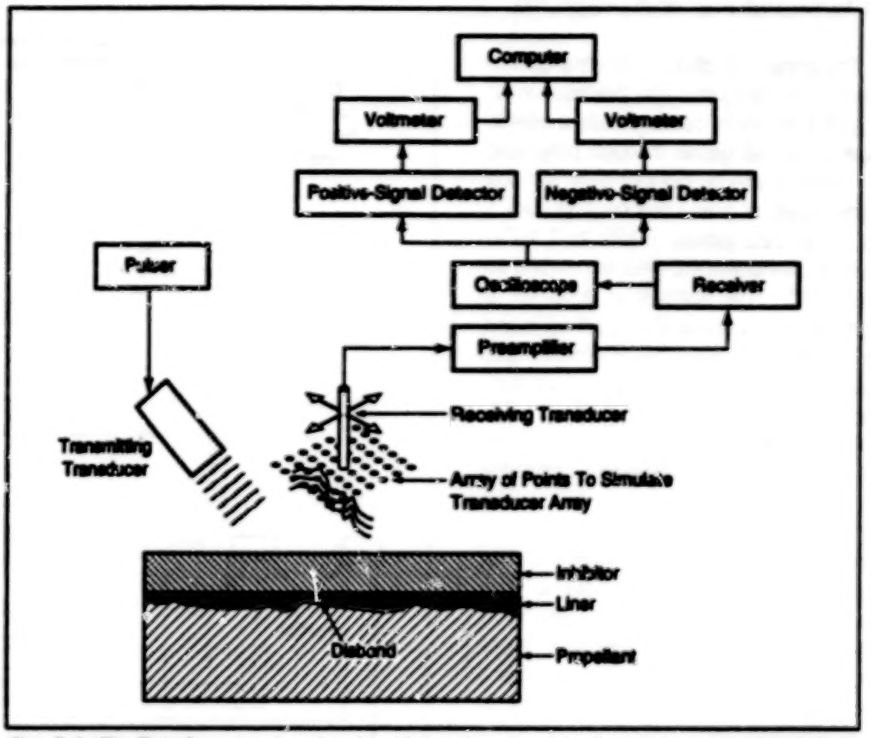

One Pointlike Receiver was translated to 49 locations in a 7-by-7 array to record signals from which a phase-insensitive image could be constructed.

To demonstrate this ultrasonic-testing concept, a prototype apparatus was constructed, using a standard ultrasonic transducer as a transmitter and a small, pointlike piezoelectric transducer as a receiver. The receiver was translated, in steps of 0.5 cm, to each of 49 locations of a 7-by-7 array on the surface of a specimen to simulate the operation of a 7-by-7 transducer array. The signals reflected from the rough interface were received, detected, recorded, and subsequently added in a phase-insensitive manner. The results were then compared with those obtained by use of a conventional pulse/echo system.

The figure illustrates the prototype apparatus. The transmitter was a 1-MHz transducer with a diameter of 1 in. (2.54 cm) and a focal length of about 4 in. (about 10 cm). (This transducer was also used in the comparative pulse/echo scan.) The receiver was a 1-MHz planar transducer with a diameter of 0.031 in. (about 0.08 cm). The transmitter was driven by a square-wave pulser, which was tuned to provide relatively sharp pulses measured at the receiver.

The signal was tuned with respect to the echo from the inhibitor-to-liner interface to account for severe attenuation in the thick inhibitor layer. Because the thickness of the inhibitor remained very nearly uniform across the ultrasonic beam, the roughness of the inhibitor did not pose a significant problem, and made it convenient to tune in this way. The transmitter and receiver were set at opposing angles of about 15° from normal and operated in a pitch/catch mode. In this configuration, the echoes could be detected in a manner similar to that of a pulse/echo system. That part of the received signal that emanated from the liner-to-propellant bondline was gated out, and the heights of signal peaks were measured. Comparison of the results showed that the conventional (pulse/echo) system was sensitive to only 42 percent of disbonds, while the prototype (phase-insensitive array) system was sensitive to 79 percent of disbonds.

This work was done by Eric I. Madaras of **Langley Research Center**. *Further information is contained in a TSP [see page 1].*

LAR-13980

Apparatus Measures Permeation of Gases Through Coupons

Permeability can be measured at a wide range of temperatures and pressures.

Lyndon B. Johnson Space Center, Houston, Texas

The apparatus shown schematically in the figure measures the permeation of any of a variety of commercially available pure or mixed gases through polymeric or other material coupons of various thicknesses at pressures ranging from 1 to 1,000 psia (about 7 kPa to 7 MPa) and temperatures ranging from −195 to +150 °C. The apparatus includes a residual-gas-analyzer (RGA) sensor head (a quadrupole mass spectrometer) and associated circuitry, and a vacuum system. The apparatus also includes a manifold with valves, through which the gas of interest can be allowed to permeate through the test coupon before traveling downstream to the evacuated RGA sensor head. The temperature of the test coupon is monitored by a thermocouple and can be maintained at a specified value above ambient by use of an electrical heating mantle or below ambient by use of a bath of ethylene glycol, water, and dry ice.

In a test, coupons are exposed continuously to the high vacuum on the downstream side and pressurized with the test gas on the upstream side. Standardized calibrated leaks containing the test gas are located on the downstream side. The gas that permeates through a given test coupon or calibrated leak is detected by the RGA sensor head, and the amount of each constituent molecular species in the gas is read directly on the digital readout of the RGA, which monitors atomic mass units from 1 to 200 on six separate channels and gives area counts for each atomic mass unit selected. This feature enables the monitoring of as many as six separate gases simultaneously, plus observation of any changes in the quantities of gases as they pass by the sensor head.

At the beginning of a test, a background reading (R_B) for the test gas is taken first on the closed vacuum system (no permeation, no calibrated leak). The valve leading to the test coupon is then opened, and the test gas at the desired pressure is applied to the coupon until equilibrium is established (typically, reaching equilibrium takes from 2 hours to 2 days, depending on the gas used). Once equilibrium is established, a reading (R_E) of the amount of gas permeating through the coupon is taken. The valve to the test coupon is then closed, the valve to a calibrated leak is opened, and after an hour, an equilibrium reading (R_L) that corresponds to the calibrated rate of leakage (L) is taken.

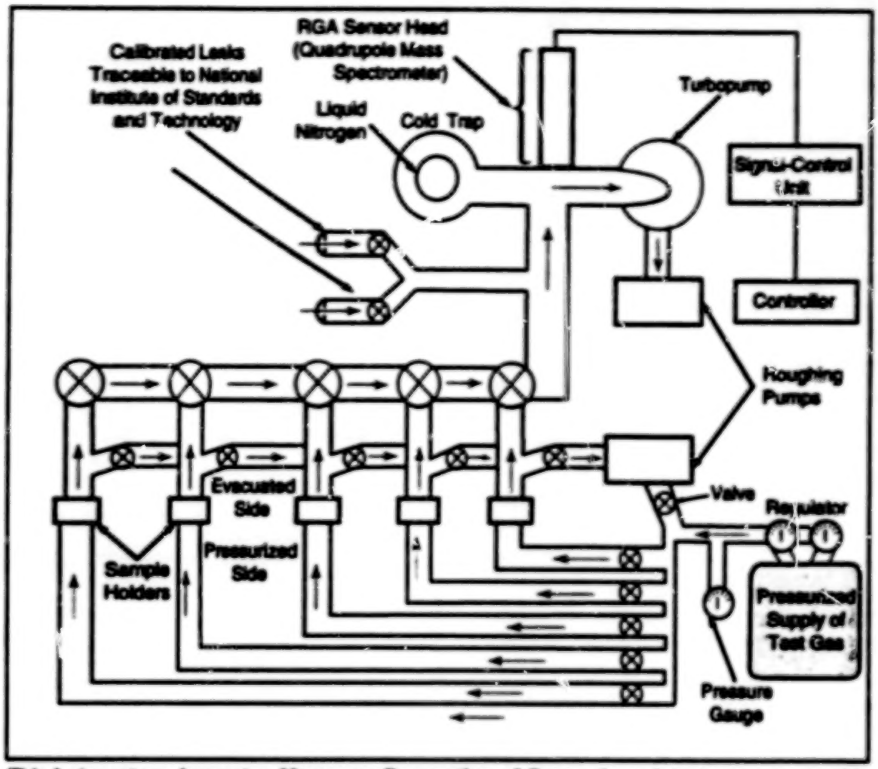

This Laboratory Apparatus Measures Permeation of Gases through test coupons, providing data that are relatively precise and reproducible in comparison with permeability data obtained by older manometric and volumetric apparatuses.

The rate of permeation (P) can then be calculated from

$$P = \left(\frac{R_E - R_B}{R_L - R_B}\right) L$$

Then a permeation-rate constant (K_p) can be calculated from the rate of permeation, the thickness (T), the test pressure (C), and area (A) of the test coupon by $K_p = PT / CA$.

This work was done by Steven J. Adam, Jim T. Morrow, and Carey E. David of McDonnell Douglas Corp. for **Johnson Space Center**. *Further information is contained in a TSP [see page 1].*
MSC-22051

Generating a Strobed Laser Light Sheet

Vortices in the wake of a model helicopter rotor are made visible.

Langley Research Center, Hampton, Virginia

An optoelectronic system that generates a synchronous, strobed sheet of laser light has been developed for use in making visible the flow of air about a model helicopter rotor. The system was used in wind-tunnel tests to determine actual locations of vortices for comparison with locations predicted by mathematical models to validate the models. Each blade tip produces a vortex. By establishing successive vortex locations, a researcher can determine the trajectory of the vortex pattern.

The light-sheet strobe circuits provided selection of blade position, strobe-pulse

duration, and multiple pulses per revolution for rotors that have two to nine blades. To make the flow visible, vaporized propylene glycol was injected upstream of the model. The system also provided calibrated trigger delay of the strobe pulse, adjustable strobe-pulse duration, selectable number of blades, and slip-sync mode to make the flow visible as though in slow motion. A calibration grid for use in extracting quantitative data was placed in the plane of the light sheet and recorded by use of the same video camera and position as those used to record the flow field.

A compound cylindrical lens assembly was used to spread the laser beam to generate a single sheet of laser light (see figure). The source of light was an argon-ion laser operating in the "all lines" mode with an output of approximately 5 W. The light sheet was strobed by the addition of an acousto-optical Bragg cell shutter, placed between the laser and the optics package, which produced zero- and first-order light beams. The zero-order beam was unused and blocked. The first-order beam from the Bragg cell was chopped by the signal being fed to the cell from the synchronization circuit.

The Bragg cell introduced color dispersion. This chromatic dispersion was corrected by the insertion of a dual prism assembly into the optical path just aft of where the beam left the Bragg cell. The dual prism assembly consisted of two rotatable prism wedges that could be adjusted to converge the different wavelengths back onto a common optical centerline.

Quantitative data were extracted by using the video record of the grid as an overlay for individual frames on the video record of the flow field. The system was used in the NASA Langley 14- by 22-ft (4.3- by 6.7-m) Subsonic Tunnel to make two-dimensional flow-field cuts of a four-bladed rotor operating at an advance ratio of 0.37 at wind-tunnel speeds up to 79.25 m/s (260 ft/s).

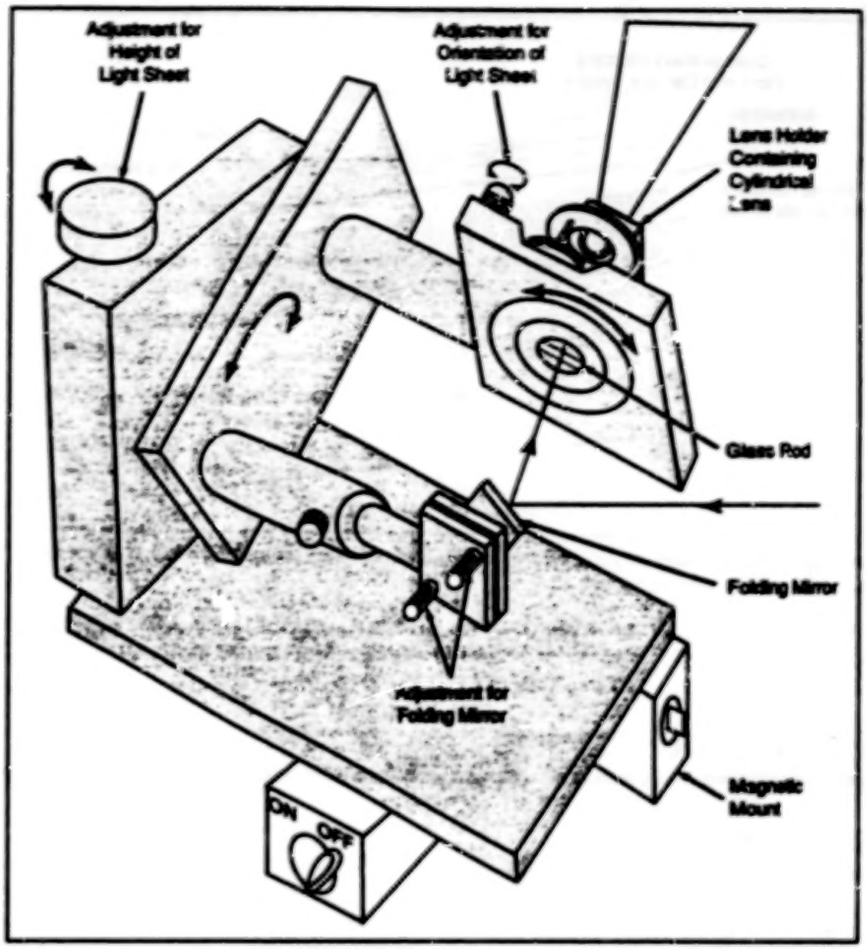

The Optical Assembly of the light-sheet-generating system was installed in the test section of a low-speed wind tunnel.

This work was done by Bradley D. Leighty, John M. Franke, David B. Rhodes, and Stephen B. Jones of **Langley Research Center.** *Further information is contained in a TSP [see page 1].*
LAR-14556

Device for Ultrasonic Scanning of Curved Object

Bristles would couple ultrasound into and out of the object.

Langley Research Center, Hampton, Virginia

The ultrasonic brush is a device that has been proposed to overcome the major difficulties that are now encountered in ultrasonic scanning of the interior of an object that has a curved surface. Unlike other scanning ultrasonic devices now in use, this device would insonify the object with uniform-phase wavefronts propagating into the interior from a relatively large area on the surface. As a result, an ultrasonic image of subsurface flaws throughout the interior could be generated much faster than in older point-excitation ultrasonic scanning and more easily than in older large-area-excitation ultrasonic scanning (in which surface curves and irregularities interfere with imaging of the interior).

The ultrasonic brush (see figure) is so named because it would include hundreds of thin, springy, coated wire bristles that would act as ultrasonic waveguides. The radius of the wire cores of the bristles would be much smaller than the wavelength of the ultrasound. The coating material and its thickness would be chosen to concentrate the sonic energy in the core and keep the waveguides isolated sonically from each other, analogously the manner in which transparent thin fiber-optic cores are coated with low-index-of-refraction material to keep the light focused in the cores.

The wires would protrude from a holder, and the free ends of the fibers would be pressed against the surface of the object to be scanned. Ultrasound would be coupled between an ultrasonic transducer and the bristles via a quarter-wave matching plate and a couplant layer on the fiber holder. Where possible, the bristles would be made of materials such that the bristles would have the same or nearly the same acoustic

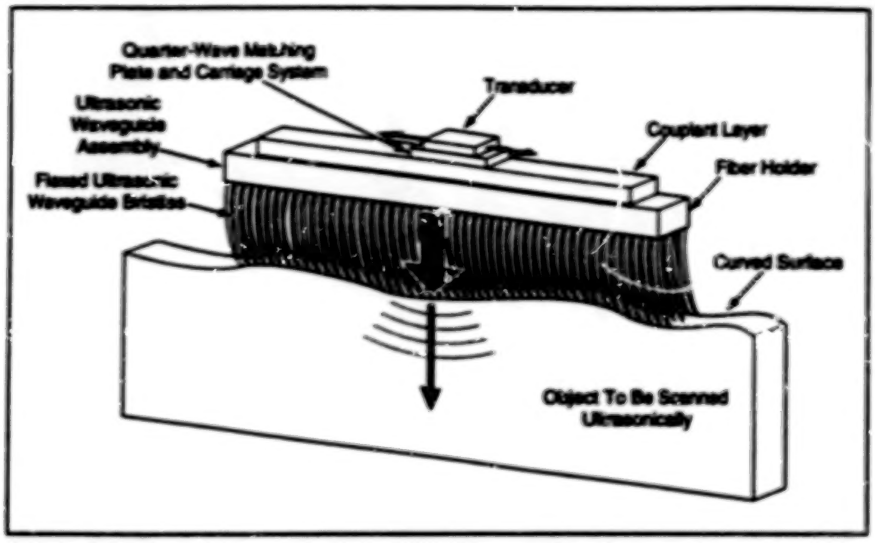

Springy Bristles would act as ultrasonic waveguides, coupling ultrasound into and out of an object through its curved surface.

impedance as that of the object to be scanned: this would provide for more efficient coupling and less spurious reflection from the surface.

The bristles would all be of the same length, so that sound generated by the transducer would arrive simultaneously at the ends of all the bristles, insonifying the object with a uniform, coherent beam propagating in from the surface. The transducer and quarter-wave plate would be moved along the couplant layer and holder to effect a B scan. In addition, the brush could be reoriented to scan in a different direction and thereby acquire data from which a three-dimensional image of subsurface flaws could be reconstructed.

This work was done by Eric Irvine Madaras of **Langley Research Center**. *No further documentation is available.*

This invention is owned by NASA, and a patent application has been filed. Inquiries concerning nonexclusive or exclusive license for its commercial development should be addressed to the Patent Counsel, Langley Research Center [see page 1]. Refer to LAR-14627.

Books and Reports

Shades Would Keep Infrared Telescope Cold

Active cooling with liquid helium would not be needed.

A report proposes the use of multiple shades to prevent solar heating of an infrared telescope in high orbit around the Earth. The shades would be part of a lightweight stowable structure that would be deployed by inflating it. The shades would be oriented so as not to interfere with the field of view of the telescope. In conjunction with a telescope design that provides for passive self-cooling by radiation to outer space in directions away from the sun, a multilayer shade design with provision for similar radiative cooling should enable the telescope to reach a low temperature in the range of 10 to 30 K. In comparison with an active cooling system based on liquid helium, this passive cooling system would be cheaper, mechanically simpler, lighter, and stowable in a smaller package. Also, the operating lifetime of the telescope would be longer because it would not be limited by depletion of the supply of liquid helium.

This work was done by Donald Rapp of Caltech for **NASA's Jet Propulsion Laboratory**. *To obtain a copy of the report, "Passive Cooling Technique for IR Observatories," see TSP's [page 1.*

In accordance with Public Law 96-517, the contractor has elected to retain title to this invention. Inquiries concerning rights for its commercial use should be addressed to

William T. Calleghan, Manager
Technology Commercialization
JPL-301-350
4800 Oak Grove Drive
Pasadena, CA 91109

Refer to NPO-19076, volume and number of this NASA Tech Briefs *issue, and the page number.*

Computing Microwave Force via Boltzmann-Ehrenfest Principle

Positioning force in microwave levitation can be determined without having to levitate a sample.

A report describes the first application of the Boltzmann-Ehrenfest principle of adiabatic invariance to prediction of the restoring force on a dielectric sphere levitated in a microwave resonant cavity in the absence of gravitation. The Boltzmann-Ehrenfest principle in this case leads to the following equation:

$\mathbf{F}(\mathbf{r}) = -(QP/\omega^2)\nabla\omega(\mathbf{r})$, where $\mathbf{F}$ is the restoring force (the springlike force on the levitated sphere toward an equilibrium levitation position), $\mathbf{r}$ is the position of the sphere, ω is the angular frequency of resonance, P is the microwave power dissipated in the cavity, and Q is the conventional resonance quality factor of the microwave cavity [2π × (the energy stored in the electromagnetic field in the cavity) ÷ (the electromagnetic energy dissipated in the cavity per cycle of oscillation)]. Thus, one need not measure the restoring force in a microwave-levitation experiment: to obtain the information needed to compute the restoring force, it suffices to measure Q, P, and ω and to measure the spatial variation of the frequency of resonance for use in computing $\nabla\omega(\mathbf{r})$. The report describes an experiment in which a microbalance was used to measure the restoring force of an alumina sphere supported on a thin quartz rod in a single-resonant-mode microwave field in a cylindrical cavity. The restoring force computed as a function of position by use of the equation agreed very well with the measured force.

This work was done by Colleen C. McDonough, Martin B. Barmatz, and Henry W. Jackson of Caltech for **NASA's Jet Propulsion Laboratory**. *To obtain a copy of the report, "Application of the Boltzmann-Ehrenfest Principle to Containerless Microwave Processing in Microgravity," see TSP's [page 1].*

NPO-19220

Diffractive Optics for Geostationary Earth Observatory

A report reviews the basic principles of diffractive optics and discusses potential uses for diffractive optical components in instrumentation to be flown in NASA's Geostationary Earth Observatory (GEO). Of course, all optics are unavoidably at least slightly diffractive, but as used here, "diffractive optics" means optical components designed specifically to exploit electromagnetic interference and diffraction, as distinguished from conventional optical components designed according to principles of ray tracing to exploit refraction and/or reflection. For example, diffractive lenses can superficially resemble Fresnel lenses (which are based on refraction), but they are more like circular diffraction gratings, with multiple focuses defined as points of convergence of light diffracted in various orders.

The report analyzes the design of the proposed GEO instruments and identifies potential applications within those instruments in which diffractive optics could improve performance while reducing weight and cost. These applications include the use of hybrid diffractive/refractive lenses in all-optic imagers (imagers to which beams of light are directed by division of the output beam of a main broadband reflective telescope), diffractive telescopes for monochromatic imaging, surfaces textured with sub-wavelength structures for antireflection and control of polarization, and diffractive components that compensate for aberrations in reflecting imaging systems and in grating spectrometers.

This work was done by G. Michael Morris, Robert L. Michaels, and Dean Fields of Rochester Photonics Corp. for **Marshall Space Flight Center**. *To obtain a copy of the report, "Diffractive Optics Technology and the NASA Geostationary Earth Observatory (GEO)," see TSP's [page 1].*
MFS-27290

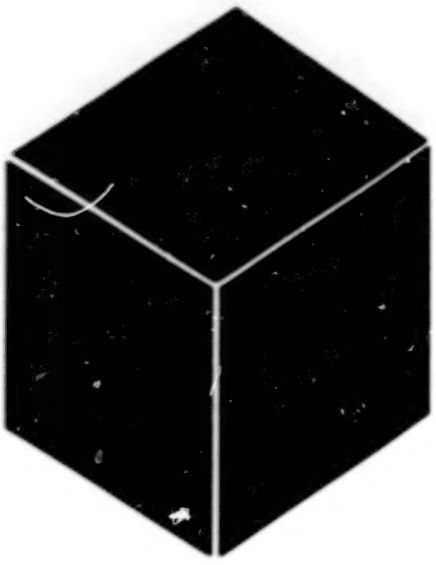

Materials

Hardware, Techniques, and Processes

27 Polyimides Made From 3,5-Diaminobenzotrifluoride
28 Intercalated-Graphite-Fiber Composites
29 Flame-Resistant Composite Materials for Structural Members

Polyimides Made From 3,5-Diaminobenzotrifluoride

Characteristics include thermo-oxidative stability, solubility in polar solvents, low dielectric constants, and transparency.

Langley Research Center, Hampton, Virginia

Polyimides have been synthesized from 3,5-diaminobenzotrifluoride (DABTF). Polyimides are an important class of polymers for use at high temperatures because they exhibit high thermo-oxidative stability. One monomer of major importance in preparing these high-temperature polymers is 1,3-phenylenediamine (mPDA). DABTF is a newly synthesized diamine derived from mPDA. DABTF contains a symmetrically substituted polar CF_3 group.

Fluorinated polyimides exhibit characteristics that make them potentially attractive for aerospace and electronic applications. These characteristics include optical transparency, solubility in common polar solvents, enhanced thermo-oxidative stability, low dielectric constants, and high glass-transition temperatures. Therefore, experiments were conducted with a view toward synthesizing polyimides with these characteristics, starting from the newly synthesized fluorinated diamine DABTF.

In the experiments, DABTF was reacted with each of the following dianhydrides: 2,2-bis (3,4-dicarboxyphenyl) hexafluoropropane dianhydride (6F); 3,3',4,4'-benzophenonetetracarboxylic dianhydride (BTDA); 4,4'-oxydiphthalic anhydride (ODPA); pyromellitic dianhydride (PMDA); 3,3',4,4'-biphenyltetracarboxylic dianhydride (BPDA); isophthaloyldiphthalic anhydride (IDPA); sulfonyldiphthalic anhydride (SO_2DPA); bis(3,4-dicarboxyphenyl)dimethylsilane dianhydride (SiDA); and 4,4'-bis(3,4-dicarboxyphenoxy)diphenylsulfide dianhydride (BDSDA).

The figure illustrates the molecular structures of DABTF and of these dianhydrides, and shows the reaction sequence. In each case, the dianhydride and DABTF monomers were dissolved in N,N-dimethylacetamide (DMAc) at a solids concentration of 20 percent, and the polymerization reaction proceeded at room temperature in the solution thus formed. The product of the reaction was a poly(amic acid), which was then thermally cyclized to convert it to the corresponding polyimide.

In comparison with the other state-of-the-art polyimides available at the time, the polyimides synthesized in these experiments were found to have greater solubility in polar solvents, less color, and lower dielectric constants. These polyimides can be used to form free-standing films, coatings, and moldings.

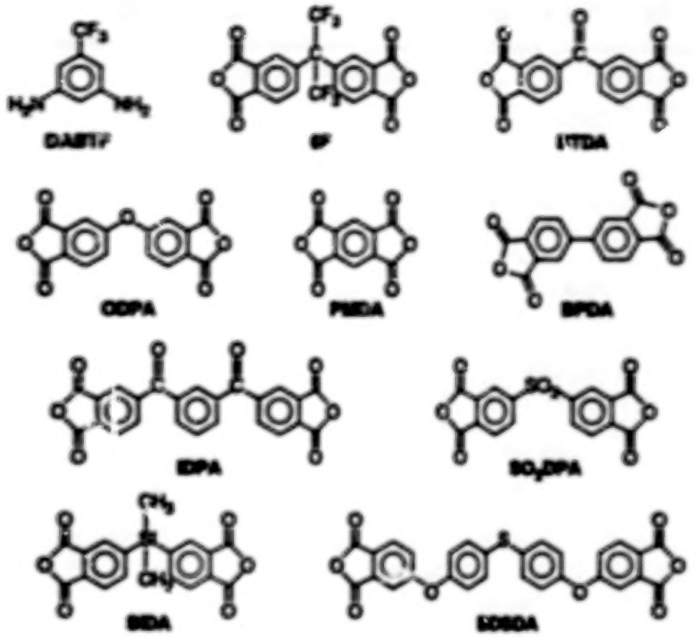

MONOMERIC INGREDIENTS

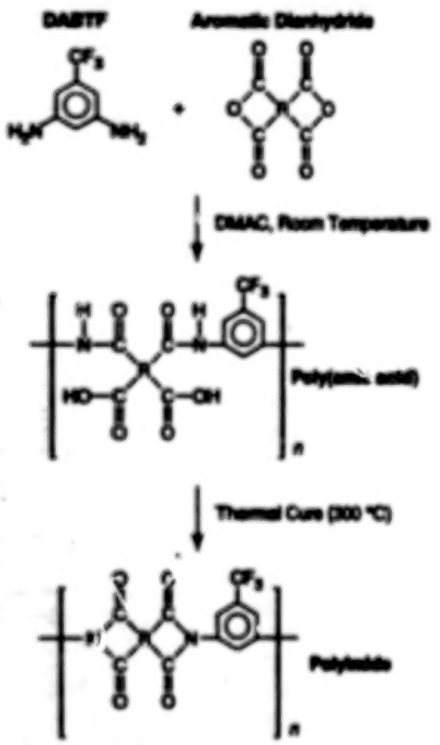

REACTION SEQUENCE

DABTF and Dianhydrides can be reacted to obtain fluorinated polyimides suitable for electronic and aerospace applications.

This work was done by Terry L. St. Clair and Anne K. St. Clair of **Langley Research Center** *and Margaret K.*

Gerber and J. Richard Pratt of Planning Research Corp. Further information is contained in a TSP [see page 1].

This invention has been patented by NASA (U.S. Patent No. 5,218,063). Inquiries concerning nonexclusive or exclusive license for its commercial development should be addressed to the Patent Counsel, Langley Research Center [see page 1]. Refer to LAR-14206.

Intercalated-Graphite-Fiber Composites

Electrically conducting composites have been made from bromine-intercalated graphite fibers in an epoxy matrix.

Lewis Research Center, Cleveland, Ohio

Although electrically conductive polymers have attracted much interest as candidate materials for incorporation into lightweight, electrically conductive composites, an alternate approach to making conductive composites is to increase the conductivities of the fibers. Carbon fibers based on polyacrylonitrile have appreciable conductivity (500 $\Omega^{-1}cm^{-1}$), and graphite fibers based on pitch have even higher conductivity (4,000 $\Omega^{-1}cm^{-1}$), but these conductivities are still well below those of common metals (10,000 to 550,000 $\Omega^{-1}cm^{-1}$). However, by intercalation (the process of introducing donor or acceptor atoms between the layers of graphite crystalline lattices), one can increase the conductivities of pitch-based graphite fibers into the metallic range (as high as 50,000 $\Omega^{-1}cm^{-1}$).

Although most elements and compounds to be intercalated into graphite are sensitive to moisture and high temperature, bromine-intercalated graphite fibers have conductivity of about 20,000 $\Omega^{-1}cm^{-1}$ and have been found to be stable in the presence of moisture (the fibers can even be submerged for indefinite times) and at reasonably high temperature (200 °C). Conventional epoxy resins, which typically require curing temperature of 175 °C, can be used with such fibers.

Composite materials that contain 50 percent bromine-intercalated graphite fibers have promising properties. The mechanical properties of such composites are similar to those of composites made with pristine fibers: The tensile and flexural strengths and the Young's and bending moduli are essentially unchanged, and the interlaminar shear strengths are slightly enhanced. The thermal conductivities of the composites also show very little degradation from those of the pristine composites. However, the electrical conductivities of the composites increase from 700 to 2,800 $\Omega^{-1}cm^{-1}$ as a result of the use of the intercalated-graphite fibers. This fourfold increase in conductivity invites the application of these composites in electrical grounding planes and in shields against electromagnetic interference.

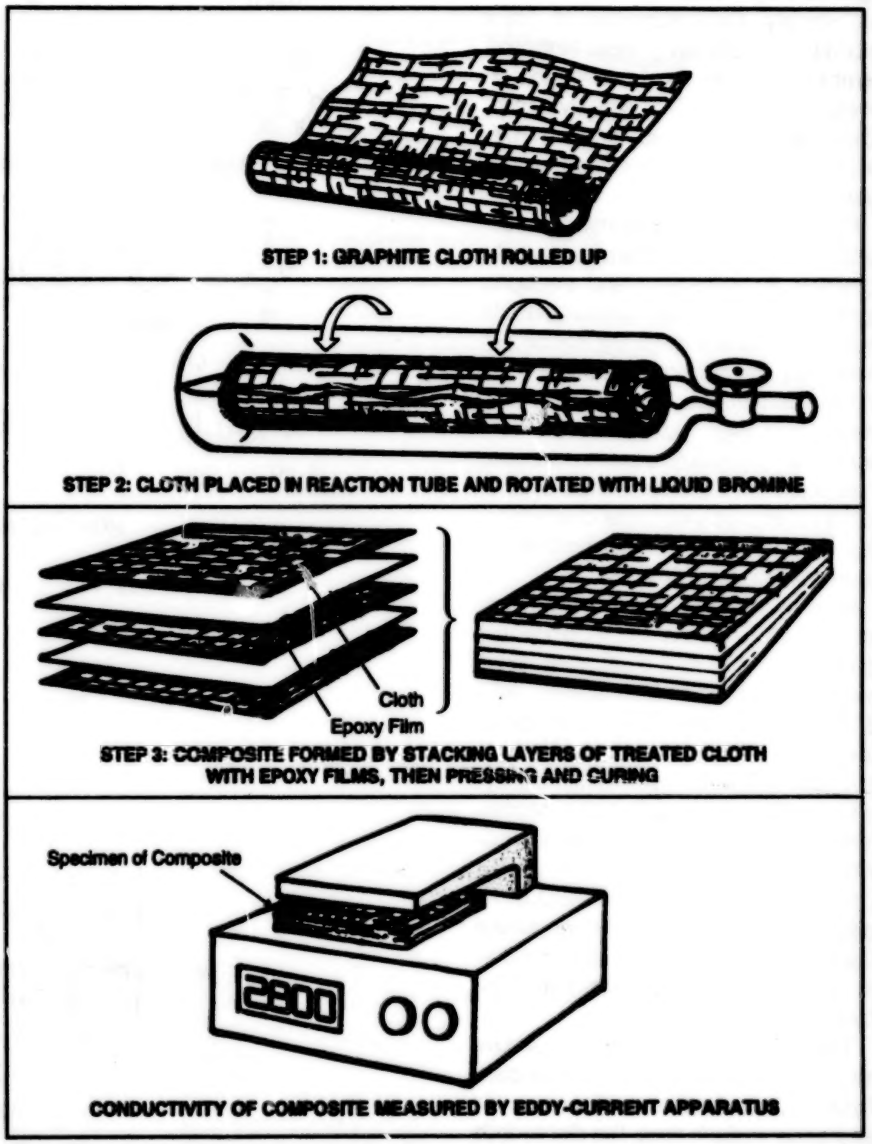
STEP 1: GRAPHITE CLOTH ROLLED UP
STEP 2: CLOTH PLACED IN REACTION TUBE AND ROTATED WITH LIQUID BROMINE
Cloth
Epoxy Film
STEP 3: COMPOSITE FORMED BY STACKING LAYERS OF TREATED CLOTH WITH EPOXY FILMS, THEN PRESSING AND CURING
Specimen of Composite
2800
CONDUCTIVITY OF COMPOSITE MEASURED BY EDDY-CURRENT APPARATUS

Bromine Is Intercalated Into Graphite-Fiber Cloth, then the cloth is used to make a fiber/epoxy composite. The electrical conductivity of the composite can be measured by use of radio-frequency eddy currents.

The intercalation process (see figure) is simple and straightforward. A cloth made of the graphite fibers is rolled up and placed into a cylindrical glass reaction tube. Liquid bromine is then introduced into the tube. The intercalation reaction occurs in both the liquid and the gas regions in the tube, though more quickly and evenly in the liquid. The tube is slowly rolled to expose every part of the graphite to the liquid. After the reaction is complete, the bromine is removed from the tube, and the cloth is washed in bromoform. This wash removes the residual bromine and lubricates the cloth so it can be easily handled and formed. A composite can then be made of the cloth and a film-type epoxy, which is cured by use of the standard procedure recommended by the epoxy manufacturer.

The determination of the electrical conductivity of a specimen of composite is not straightforward because the conducting fibers are embedded in the insulating matrix. A contactless radio-frequency eddy-current technique, of the type used in the semiconductor industry, has been used to characterize specimens of this type. Although this technique avoids the difficult problem of how to make contact, the electrical conductivity of the composite has a complicated directionality, which cannot be measured by this technique. Currents that flow along the fibers flow approximately like those in parallel conductors and can be treated by a simple rule-of-mixtures mathematical model. Currents that travel in other directions must percolate from fiber to fiber through the insulating matrix. The conductivity measured by use of radio-frequency eddy currents is about half that measured in the fibers and predicted by a simple rule of mixtures.

This work was done by James R. Gaier of **Lewis Research Center** *and Paul D. Hambourger and Melissa E. Coan of Cleveland State University. Further information is contained in a TSP [see page 1].*

This invention has been patented by NASA (U. S. Patent No. 5,073,412). Inquiries concerning nonexclusive or exclusive license or its commercial development should be addressed to the Patent Counsel, Lewis Research Center [see page 1]. Refer to LEW-15077.

Flame-Resistant Composite Materials for Structural Members

Surface layers of ceramic fabric are integrated into the members.

John F. Kennedy Space Center, Florida

Matrix/fiber composite materials are being developed for structural members that are occasionally exposed to hot, corrosive gases. In the original intended application, the composite members would replace steel structural members of rocket-launching structures that deteriorate under the combined influences of the atmosphere, spilled propellants, and rocket exhaust. The composites may also be attractive for other applications in which corrosion- and fire-resistant structural members are needed.

A typical composite-material member considered in this development work comprises a phenolic or other heat-resistant thermosetting resin reinforced by internal layers of glass fabric, plus a surface layer of ceramic fabric that is molded together with the internal layers and matrix material into a single, integral piece (see figure). The ceramic-fabric surface layer resists flames, protects against erosion, provides strength, and resists chemicals. By so doing, it retards deterioration of the entire underlying composite material.

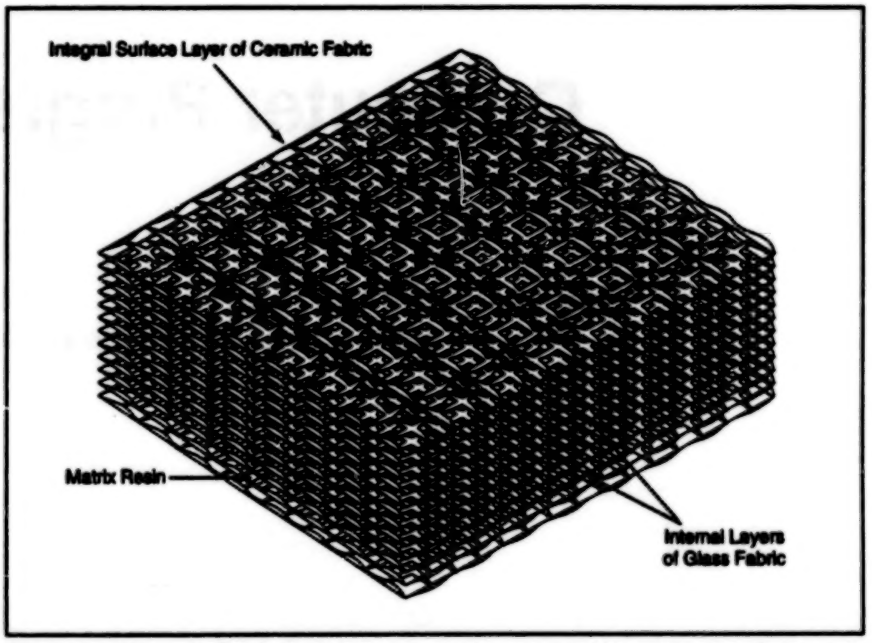

The Integral Ceramic Fabric Surface Layer would be essential for resistance to flames and chemicals. This layer endures high temperature, impedes a flame from penetrating to the interior, inhibits the diffusion of oxygen to the interior where it would degrade the matrix resin, resists attack by chemicals, helps to resist erosion, and provides additional strength.

Experimental composite specimens have been made by resin-transfer molding, but in production, the composite structural members would likely be made by pultrusion. Further work must be done to develop the parameters of a pultrusion process. Until now, high volume production pultrusion, in which reinforcement fibers are impregnated with resin and fed to forming and curing dies, has been confined to polyesters, vinyl esters, and epoxies. The pultrusion process will have to be adapted to phenolic resins, and this requires study of the temperatures, viscosities, and curing characteristics of phenolic formulations.

This work was done by Richard K. Spears of Largo Scientific, Inc., for **Kennedy Space Center**. *Further information is contained in a TSP [see page 1].*
KSC-11613

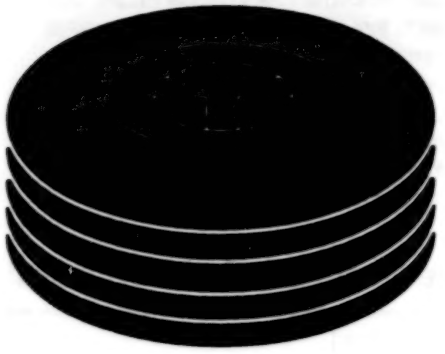

Computer Programs

Physical Sciences

31 Computer Model of Fragmentation of Atomic Nuclei

Computer Programs

These programs may be obtained from COSMIC. Please contact

COSMIC®
Computer Services Annex
University of Georgia
Athens, GA 30602
Telephone No. (404) 542-3265.

Physical Sciences

Computer Model of Fragmentation of Atomic Nuclei

This semiempirical model accounts for the principal physical effects.

The High Charge and Energy Semiempirical Nuclear Fragmentation Model (HZEFRG1) computer program was developed to be a computationally efficient, user-friendly, physics-based program for generating data bases on the fragmentation of atomic nuclei. (The "Z" in "HZE" is the customary mathematical symbol for the number of units of positive charge in an atomic nucleus; hence, "HZE" signifies "high charge and energy.") The data bases generated by HZEFRG1 can be used in calculations that pertain to such radiation-transport applications as shielding against radiation in outer space, radiation dosimetry in outer space, cancer therapy in laboratories with beams of heavy ions, and simulation studies for designing detectors for experiments in nuclear physics. The program provides cross sections for production of individual elements and isotopes in breakups of high-energy heavy ions by the combined nuclear and Coulomb fields of the interacting nuclei.

In HZEFRG1, the contributions to breakups of nuclei are estimated by use of an energy-dependent, abrasion/ablation mathematical model of fragmentation of heavy ions. The abrasion step involves removal of nucleons by direct knockout in the region of overlap of the colliding nuclei. The abrasions are treated on a geometric basis, and uniform spherical distributions of densities in nuclei are assumed. Empirical radii of nuclei obtained from tabulations of electron-scattering data are incorporated. Nuclear-transparency effects are included by use of an energy-dependent, impact-parameter-dependent average transmission factor for the projectile and target nuclei, which factor accounts for the finite mean free paths of nucleons in nuclear matter.

The ablation step, as implemented by Bowman, Swiatecki, and Tsang (LBL report LBL-2908, July 1973), is treated as an emission of a single nucleon for every 10 MeV of excitation energy. Contributions to fragmentation from electromagnetic dissociation processes that arise from the interacting Coulomb fields are estimated by use of the Weiszacker-Williams theory, extended to include the contributions of electric dipoles and quadrupoles to the cross sections for removal of single nucleons.

HZEFRG1 consists of a main program, seven function subprograms, and thirteen subroutines. Each subprogram and subroutine is fully explained by comments contained within it and begins with a brief description of its functionality. The inputs, which are provided interactively by the user in response to questions displayed on the computer video screen, consist of the energies of the projectile nuclei in units of MeV/nucleon and the masses and charges of the projectile and target nuclei. With proper inputs, HZEFRG1 first calculates the cross sections for electromagnetic dissociation and then begins the calculations of fragmentation of nuclei by searching through a specified number of isotopes for each charge number (Z) from Z=1 (hydrogen) to the charge of the incident fragmenting nucleus (Z_p). After computing the cross sections for fragmentation of the nuclei, HZEFRG1 sorts through the results and writes the sorted output to a file in descending order, based on the charge numbers of the fragmented nuclei. Details of the theory that underlies the computer code, extensive comparisons of its predictions with available experimental cross-section data, and a complete description of the computer code are given in the program documentation.

HZEFRG1 is written in ANSI FORTRAN 77 to be machine-independent. It was originally developed on a DEC VAX-series computer, and has been successfully implemented on a DECstation computer running RISC ULTRIX 4.3, a Sun4-series computer running SunOS 4.1, an HP 9000-series computer running HP-UX 8.01, a Cray Y-MP-series computer running UNICOS, and IBM PC-series computers running MS-DOS 3.3 and higher. HZEFRG1 requires 1MB of random-access memory for execution. In addition, a FORTRAN 77 compiler is required to create an executable code. A sample output run is included on the distribution medium for numerical comparison. The standard medium for distribution of this program is a 3.5-in. (8.89-cm), 1.44MB MS-DOS-format diskette. Alternate distribution media and formats are available upon request. HZEFRG1 was completed in 1992.

This program was written by John W. Wilson and Lawrence W. Townsend of **Langley Research Center** *and Ram K. Tripathi of Vigyan, Inc., John W. Norbury of Rider College, Ferdous Khan of Old Dominion University, and Francis F. Badavi of Christopher Newport University. Further information is contained in a TSP [see page 1].*
LAR-15230

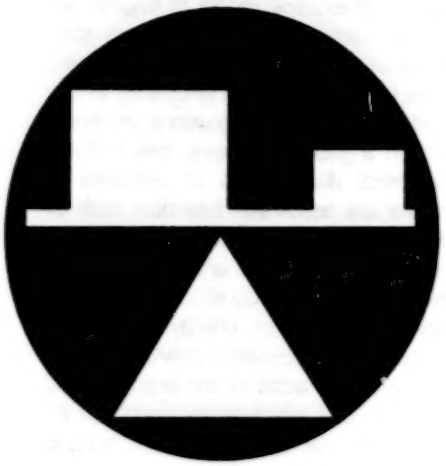

Mechanics

Hardware, Techniques, and Processes

33 Blending Velocities in Task Space in Computing Robot Motions

34 Calculating 3-D Crack-Opening Behavior of a Fatigue Crack

Blending Velocities in Task Space in Computing Robot Motions

The computational burden is less than that of blending positions and orientations.

NASA's Jet Propulsion Laboratory, Pasadena, California

Blending of linear and angular velocities between sequential specified points in task space constitutes the theoretical basis of an improved method of computing trajectories to be followed by robotic manipulators. Task space denotes the coordinate transformation describing the end-effector position and orientation, as well as other parameters (e.g., arm angle, base position) which completely and conveniently describe the arm pose without explicit specification of the joint angles. A related prior method of generating trajectories involves blending of positions and orientations between sequential points in task space. The present improved method achieves the same results as does the prior method, but with much less computation.

In the improved method, a generalized velocity-vector-blending technique provides a relatively simple, common conceptual framework for blending linear, angular, and other parametric velocities. The velocity vectors originate from straight-line segments that connect the specified task-space points, which are called "via frames" and which represent specified robot poses (see figure). Linear-velocity-blending functions can be chosen from among first-order, third-order-polynomial, and cycloidal options (see figure). Angular velocities are blended by use of a first-order approximation of a previous orientation-matrix-blending formulation. The angular-velocity approximation yields a small residual error, which is quantified and corrected.

The method was tested, both by computer simulation and by experimentation on a computer-controlled seven-degree-of-freedom robot arm on a one-degree-of-freedom platform, as shown in simplified form in the figure. Linear blending was arbitrarily chosen for these tests. The results of both the simulation and experiments showed that the method offers both the relative simplicity and the speed needed for generation of robot-manipulator trajectories in real time.

This work was done by Richard A. Volpe of Caltech for **NASA's Jet Propulsion Laboratory.** *Further information is contained in a TSP [see page 1].*

This invention is owned by NASA, and a patent application has been filed. Inquiries concerning nonexclusive or exclusive license for its commercial development should be addressed to the Patent Counsel, NASA Resident Office–JPL [see page 1]. Refer to NPO-19022.

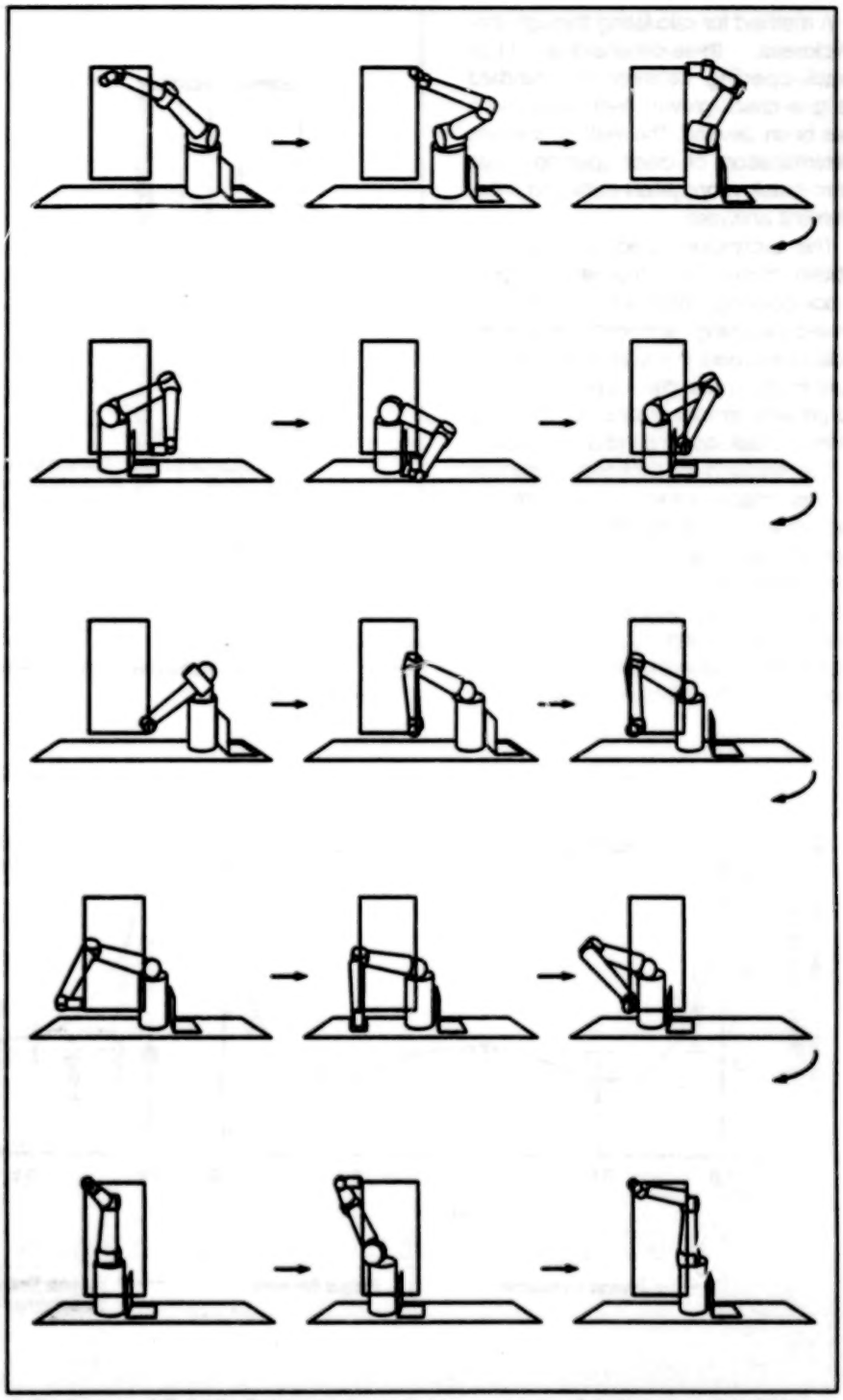

A Sequence of Robotic Poses corresponds to a sequence of task-space points between which velocity vectors are defined. The velocities are then blended according to the improved method to obtain a smoothed trajectory. In this case, the robotic manipulator is commanded to move through a sequence of specified poses to inspect a rectangular object.

Calculating 3-D Crack-Opening Behavior of a Fatigue Crack

Predicted values of fatigue-crack-opening loads are close to experimental values.

Langley Research Center, Hampton, Virginia

A method for calculating through-the-thickness, three-dimensional (3-D) crack-opening behavior in standard fatigue-crack-growth test specimens has been devised. The method involves determination of crack-opening loads from crack-propagation data and finite-element analyses.

The techniques used heretofore to obtain through-the-thickness fatigue-crack-opening behaviors are complex, time-consuming, and entail considerable investment in equipment. The present method was developed in an effort to provide simpler means for obtaining fatigue-crack-opening behavior loads.

The through-the-thickness variations in the crack-opening stress-intensity factors are calculated from a combination of experimental data and finite-element computations. In this method, one considers (1) the variation in the rate of crack growth along a crack front, (2) the relationship between the rate of crack growth and the effective stress intensity

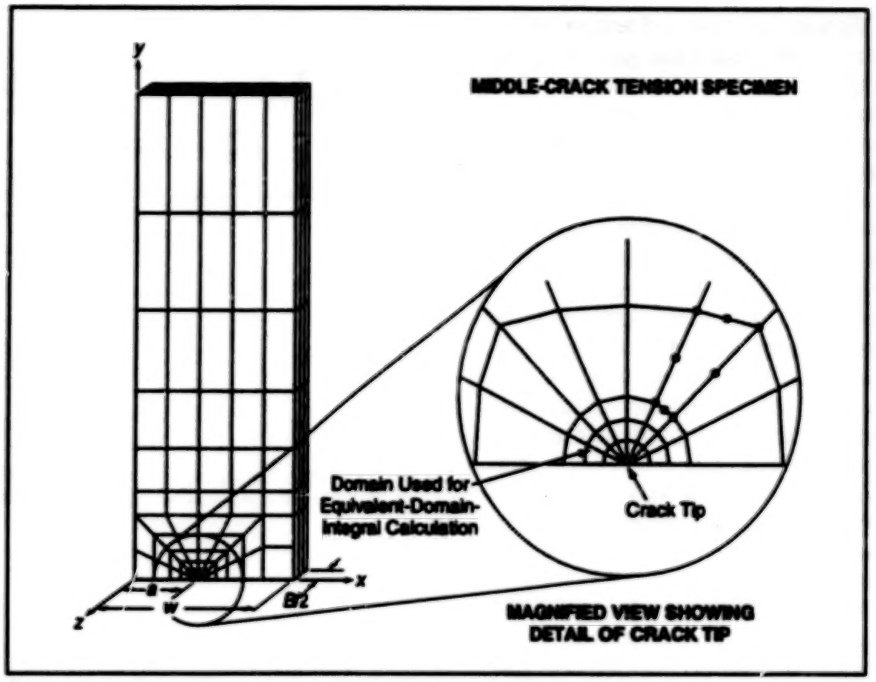
MIDDLE-CRACK TENSION SPECIMEN
Domain Used for Equivalent-Domain-Integral Calculation
Crack Tip
MAGNIFIED VIEW SHOWING DETAIL OF CRACK TIP

Figure 1. A Three-Dimensional Finite-Element Model is used to calculate crack-front stress-intensity factors.

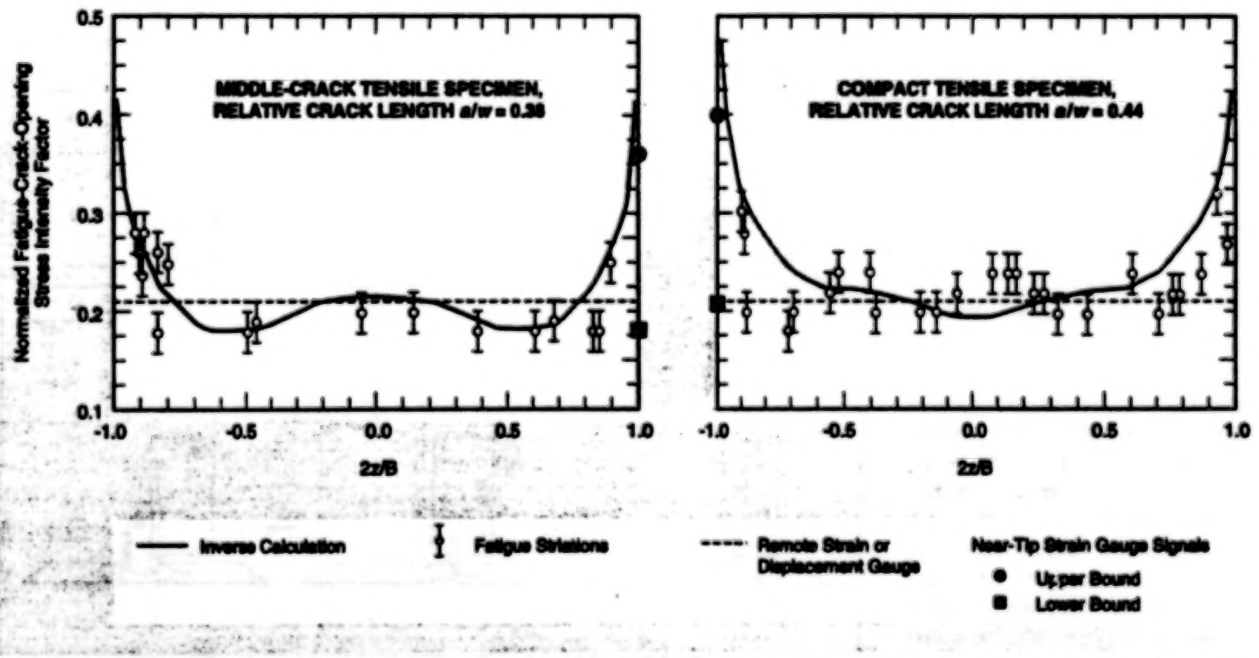
MIDDLE-CRACK TENSILE SPECIMEN, RELATIVE CRACK LENGTH a/w = 0.38
COMPACT TENSILE SPECIMEN, RELATIVE CRACK LENGTH a/w = 0.44
Normalized Fatigue-Crack-Opening Stress Intensity Factor
2z/B
Inverse Calculation
Fatigue Striations
Remote Strain or Displacement Gauge
Near-Tip Strain Gauge Signals
Upper Bound
Lower Bound

Figure 2. Theoretical and Experimental Values of through-the-thickness variations of fatigue-crack-opening stress-intensity factors for two specimen types are shown.

factor, and (3) the variation in the three-dimensional stress-intensity factor along the crack front.

The variation in the rate of crack growth is obtained by comparison of experimentally observed changes in the crack front. The relationship between the rate of crack growth and the effective stress-intensity factor is estimated from data obtained in high-stress-ratio, constant-load-amplitude fatigue-crack-growth tests. The variation in the three-dimensional stress-intensity factor along the crack front is computed as a function of the stress ratio and a normalized crack-opening load (among other quantities) by use of a mathematical model developed previously. The through-the-

thickness variation of the effective stress-intensity factor for a specific crack observed experimentally is computed by use of the three-dimensional equivalent-domain-integral method in conjunction with a finite-element mathematical model of the specimen and crack (see Figure 1).

Figure 2 presents examples of through-the-thickness variations of normalized fatigue-crack-opening stress-intensity factors as calculated by the method and as determined experimentally by use of fatigue striations, near-tip strain gauges, remote (back-face) strain gauges, and remote displacement gauges. In both examples, the values calculated appear in reasonable agreement with the experimental values.

This work was done by J. C. Newman, Jr., of **Langley Research Center**, *D. S. Dawicke and K. N. Shivakumar of Analytical Services and Materials, Inc., and A. F. Grandt, Jr., of Purdue University. Further information is contained in a TSP [see page 1].*
LAR-14598

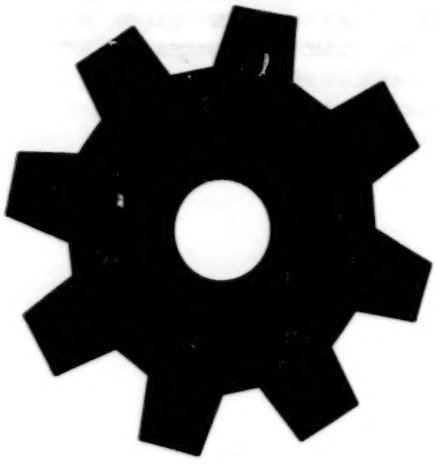

Machinery

Hardware, Techniques, and Processes

37 Supersonic-Spray Cleaner
38 Stabilizing Gas Bearings in Free-Piston Machines
39 Heat-Transfer Head for Stirling-Cycle Machine
40 Power Tool Would Require Little Bracing Torque

Books and Reports

40 Magnetic Bearings for Turbopumps

Supersonic-Spray Cleaner

A reduced amount of liquid is needed.

John F. Kennedy Space Center, Florida

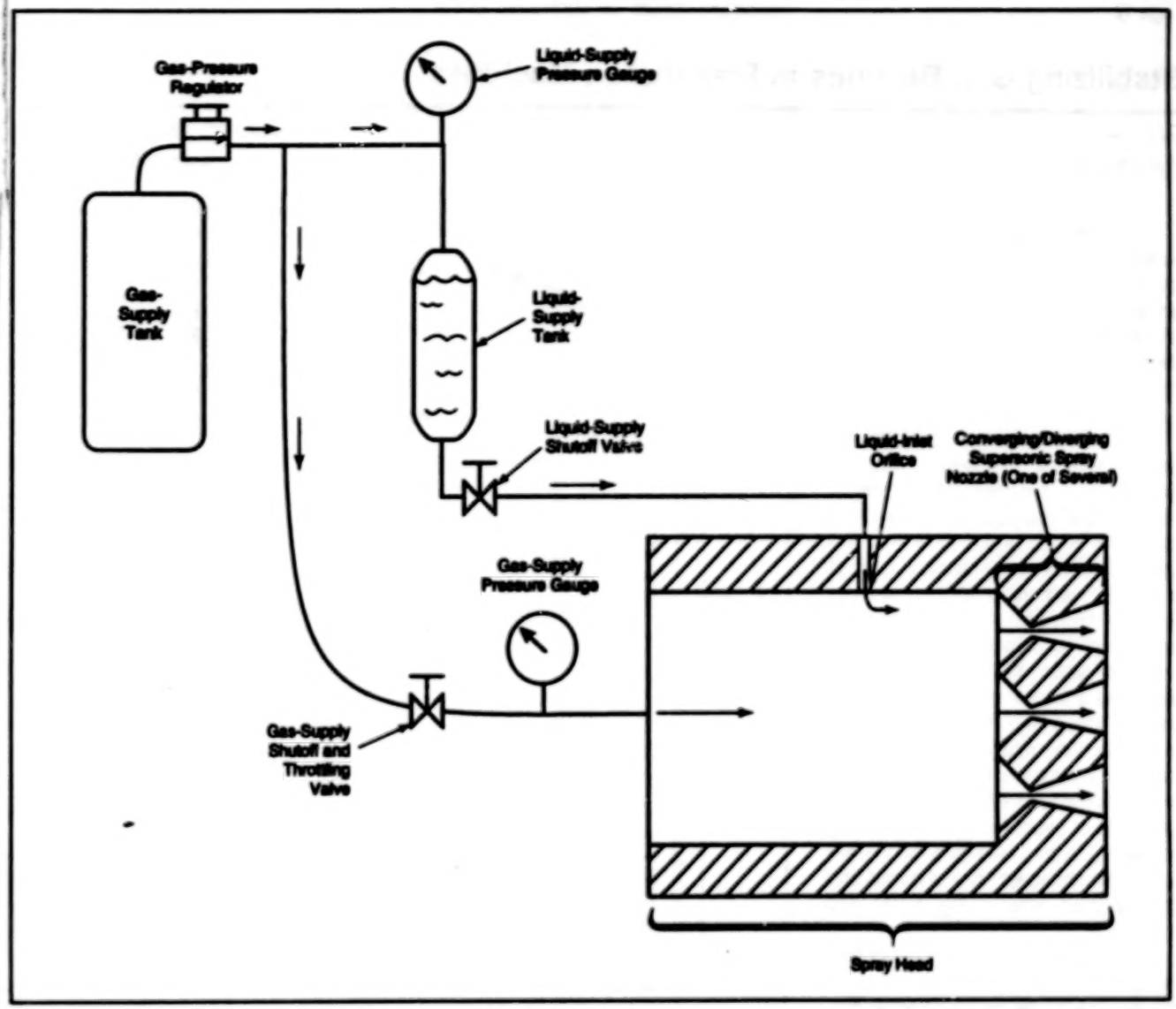

The Liquid/Gas Mixture Is Accelerated in the Nozzles to supersonic velocity. The gas serves as a pressurizing agent for the liquid tank and as a transport medium for the liquid.

A spraying system for cleaning mechanical components uses less liquid than does a typical older spray cleaner of similar capability, and it operates at pressures significantly lower than those of conventional pressure washers. The lower consumption of liquid helps alleviate the problem of safe disposal. The liquid currently being used at KSC is water. This system was designed to replace the chlorofluorocarbon (CFC) solvent-based cleaning and cleanliness verification methods. (CFC's contribute to the depletion of ozone from the stratosphere.)

The system imparts a supersonic velocity to a stream of liquid, giving the liquid droplets sufficient kinetic energy to dislodge contaminants and carry them off. The system consists of a spray head containing supersonic converging/diverging nozzles, a source of gas at regulated pressure, a pressurized liquid tank, and various hoses, fittings, valves, and gauges (see figure). The gas flows through a throttling valve to the spray head. The liquid is injected into the flowing gas through an orifice in the spray head just upstream of the nozzles. The liquid/gas mixture enters the nozzles, wherein the flow accelerates it to supersonic speed. The supersonic flow from the nozzle is directed at the part to be cleaned.

The parameters of the nozzles can be set so that any of a large variety of liquids and gases can be combined in the desired ratio and rate of flow. The size and number of nozzles can be varied so that the system can be built in configurations that range from small hand-held spray heads to large multinozzle cleaners.

The system can also be used to verify that a part has been adequately cleaned. Runoff liquid from the spray directed at the part is collected. The liquid is analyzed for the presence of contaminants, and the part is recleaned if necessary.

This work was done by Raoul E. B. Cairni, Feng-Nan Lin, and Eric A. Thaxton of **Kennedy Space Center.** *Further information is contained in a TSP [see page 1].*

This invention is owned by NASA, and a patent application has been filed. Inquiries concerning nonexclusive or exclusive license for its commercial development should be addressed to the Patent Counsel, Kennedy Space Center [see page 1]. Refer to KSC-11641.

Stabilizing Gas Bearings in Free-Piston Machines

Grooves and drain galleries reduce undesired dynamic loads.

Lewis Research Center, Cleveland, Ohio

Gas bearings and clearance seals between pistons and cylinders in free-piston machines can be designed to reduce undesired dynamic forces and torques on the pistons, gas bearings, and cylinders. This stabilization can be achieved without significant adverse effect on performance.

Free pistons with gas bearings are used in long-life Stirling-cycle engines. Each free piston reciprocates between a gas spring at one end and the working gas of the engine at the other end. The gas spring provides reactive flow of power (in mechanical analogy to reactive flow of power in electrical capacitors and inductors), alternately accelerating and decelerating the piston. The clearance seal isolates the pressure waves in the gas spring from the pressure waves in the working space. Because these pressure waves are not in phase with each other, they give rise to time-varying gradients of pressure across and along the seal. The gradients give rise to leakage (with consequent loss of power) and to unwanted time-varying forces and torques.

The undesired dynamic loads are proportional to the length of the seal, while the leakage power loss is inversely proportional to the length. Therefore, in prior designs, it was necessary to sacrifice efficiency to reduce undesired dynamic loads, or vice versa. The improved design provides stabilization without significant reduction in the length of the seal and, therefore, without significant increase in leakage and the consequent reduction of efficiency.

One principal feature of the improved design is the incorporation of circumferential grooves into either the inner wall of the cylinder or the mating surface of the piston (see figure). The optimum number and dimensions of the grooves depend on other geometric parameters of the gas bearings/seals, the frequency of reciprocation, and the magnitude of the pressure gradient. In general, the groove should be large enough to ensure uniform pressure around its circumference, yet small enough that the time needed to fill it is a small fraction of the period of reciprocation.

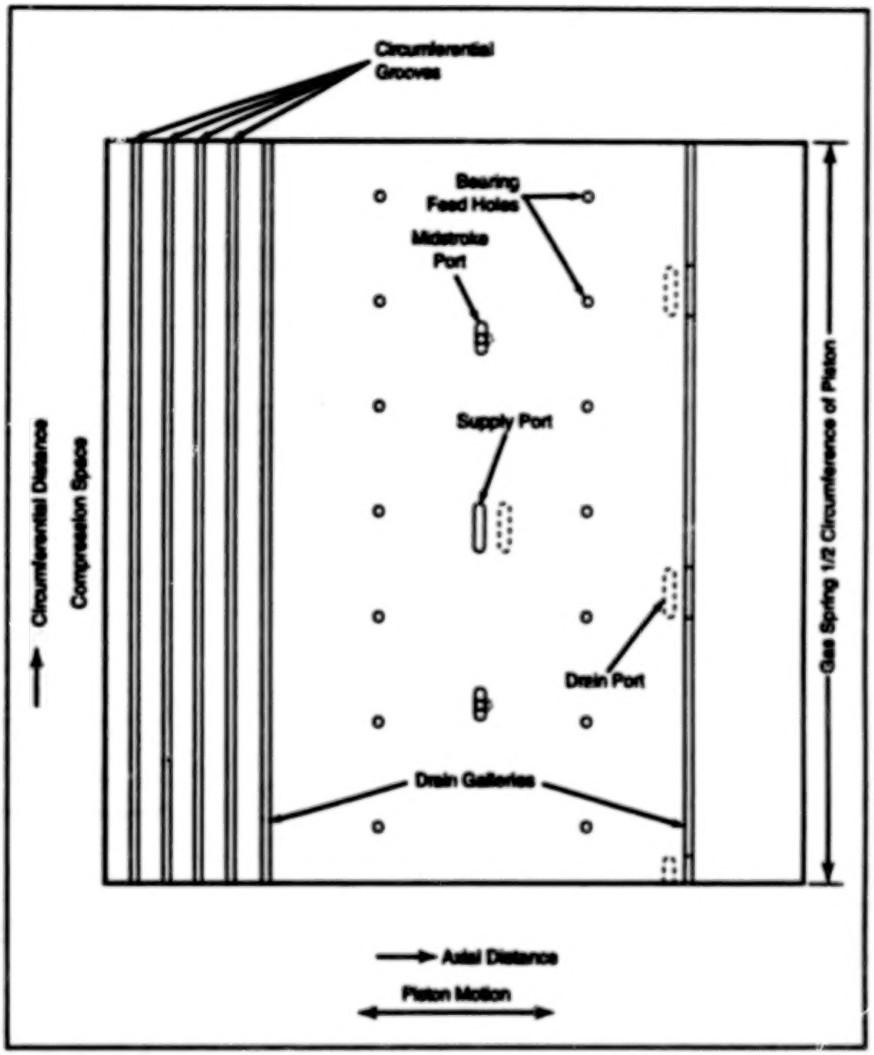

Circumferential Grooves and Drain Galleries are added to the piston or cylinder in the improved design.

To suppress angular oscillations of the piston and cylinder relative to each other, it is necessary to isolate the pressure waves in the working gas and in the gas spring from the gas bearing. For this purpose, drain galleries are provided. These galleries connect some of the grooves with a mean-pressure volume in the engine.

This work was done by Manmohan Dhar of Mechanical Technology, Inc., for **Lewis Research Center.** *Further information is contained in a TSP [see page 1].*
LEW-15122

Heat-Transfer Head for Stirling-Cycle Machine

Two heat acceptors are replaced by the single heat-transfer head.

Lewis Research Center, Cleveland, Ohio

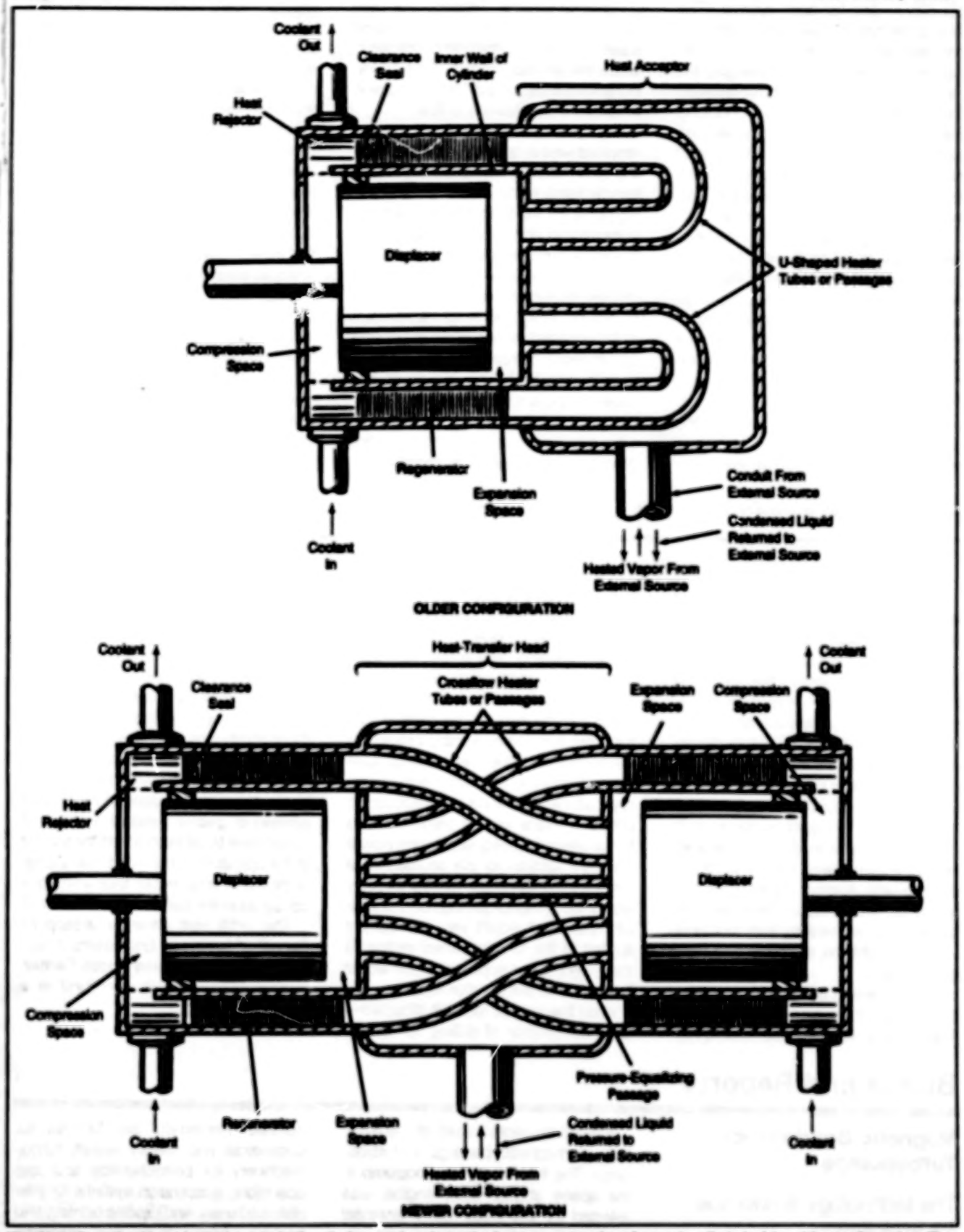

The Heat-Transfer Head is common to both cylinders and replaces the heat acceptors (one for each cylinder) of the older configuration. The heat-transfer head offers less resistance to the flows of heat and of working gas than the previous heat acceptors do.

A new common heat-transfer head for the two cylinders of an opposed-cylinder Stirling-cycle machine performs the function formerly performed by two heat acceptors — one for each cylinder. (The heat acceptors are heat exchangers that are described more fully below.) The heat-transfer head was invented to simplify the structure of the machine and to increase the efficiency of operation by (1) reducing the resistance to the flow of the working gas and/or (2) increasing the transfer of heat to or from the working gas during its flow between the compression and expansion spaces of the machine.

The Stirling-cycle machine can be a heat engine or a heat pump. The upper part of the figure gives a simplified view of one cylinder of such a machine in an older configuration. A displacer (essentially a piston) slides axially back and forth past a clearance seal in the cylinder, interacting with the working gas in the compression and expansion spaces. As the working gas flows between the compression and expansion spaces of the cylinder, it passes through three heat exchangers: the heat acceptor, the regenerator, and the heat rejector. Within the heat acceptor, the working gas exchanges substantial amounts of heat with an external source. Typically, the heat acceptor contains elongated, U-shaped tubes or other heat-transfer passages in which the direction of flow of the working gas must be turned 180°; this turning increases the resistance to flow.

The lower part of the figure gives a simplified view of an opposed-piston Stirling-cycle machine with a common heat-transfer head. In this machine, the working gas is not made to flow between the compression and expansion spaces of the same cylinder, and it is not necessary to turn the flow 180° in a heat exchanger. Instead, the common heat-transfer head is configured to take advantage of the opposed motion of the displacers (simultaneous compression or expansion in both cylinders). The gas flows between the expansion space of one cylinder and the compression space of the other cylinder along a path that includes crossflow heater tubes or passages in the heat-transfer head.

In comparison with the U-shaped heater tubes or passages in a heat acceptor, the crossflow heater tubes or passages are more nearly straight, with consequent lower resistance to flow. Compared to another opposed-cylinder design that uses straight tubes for the heat acceptors, the crossflow arrangement reduces the dead volume in the expansion space, yielding improved specific power. Although the crossflow paths are shown as simple tubes in the figure, the passages in a practical and efficient design would more likely be incorporated into and between integral structural ribs, and the ribs and passages would be optimized with respect to considerations of flow, transfer of heat, and the size and shape of the cylinders.

This work was done by Stuart G. Emigh, Gregory A. Lehmann, and Jack E. Noble of Stirling Technology Co. for the Power Technology Division of **Lewis Research Center**. *Further information is contained in a TSP [see page 1].*
LEW-15270

Power Tool Would Require Little Bracing Torque

Torque would be reacted internally.

Lyndon B. Johnson Space Center, Houston, Texas

A proposed rotary power tool would exert the required torque on the workpiece (e.g., to turn a drill bit), but little or no bracing torque would have to be applied to the tool to keep it from turning in the opposite direction. Instead, the working torque would be neutralized by a nearly equal and opposite torque generated within the tool. In comparison with a conventional rotary power tool, the proposed tool could be used more easily underwater, on slippery surfaces, or in other environments in which external bracing of the tool against rotation is difficult or impossible. Another benefit of this tool would be that it would minimize arm-breaking forces resulting from tool binding (i.e., a drill bit suddenly becoming locked up).

The tool would be based on the reaction-wheel, or countertorque, concept. The tool drive would contain electric motors, the frames of which would be connected back to back. The frames could be isolated (with respect to torque) from the tool housing. The armatures of the two motors would be made to turn in opposite directions. One of the motors would turn the tool bit; the other would turn a reaction wheel, possibly through an electromagnetic clutch (depending upon the application). In the case of high-torque applications, power could be applied to only one motor until a predetermined torque was exceeded, whereupon power could be applied to the countertorque motor/clutch assembly. Control circuitry would sense the torque load on the tool-bit motor and would vary the current applied to the reaction-wheel motor so that an equal but opposite torque would be applied to the reaction wheel.

When the tool-bit motor is stopped — upon completion of drilling, for example — the kinetic energy accumulated in the reaction wheel and its motor would be dissipated by allowing the reaction wheel and its motor to coast to a stop via bearing friction. The torque transmitted to the operator's hand or tool-holding jig via bearing friction would be low. Alternatively, the reaction-wheel motor could be connected to a static load (in effect, a brake) that would absorb the kinetic energy faster, albeit at the price of somewhat greater residual torque that would have to be reacted via the tool bit or the operator's hand — but over a longer period of time, rather than instantaneously as in the case of a sudden bind.

This work was done by Joseph H. Cannill of Lockheed Engineering & Sciences Co. for **Johnson Space Center**. *Further information is contained in a TSP [see page 1].*
MSC-22153

Books and Reports

Magnetic Bearings for Turbopumps

The technology is now ripe for exploitation.

A report presents a study of the feasibility of magnetic bearings in turbopumps. The liquid-oxygen turbopump in the space shuttle main engine was selected for the study. Other potential applications include manned and unmanned spacecraft, gas turbines for commercial and military aircraft, turbomachinery for petrochemical and gas operations, suspension systems for precise machinery, and precise pointing and tracking systems. In the past, magnetic

bearings and their controls have been too large, heavy, and power consuming to be considered seriously for most applications. That view has now been changed by technological advances in permanent-magnet and ferromagnetic materials, rotor-position sensors, and compact electronic circuits for controlling electromagnets. In the study, candidate magnetic-bearing systems were evaluated on the basis of the need to minimize size, weight, and power. The preferred approach was found to involve a homopolar, permanent-magnet bias, electromagnet-control magnetic bearing. The selected concept was optimized by a computer-aided design program. A preliminary analysis of rotor dynamics was performed, and designs for the control system and position sensor were considered. High-temperature-superconducting magnetic bearings were evaluated and found to be impractical for the near term because they are still too heavy and necessitate too complicated a startup procedure.

This work was done by Crawford R. Meeks and Antonio J. Mendez of Avcon-Advanced Controls Technology, Inc., for **Marshall Space Flight Center**. *To obtain a copy of the report, "Innovative Magnetic Suspension Technology for Space Shuttle Main Engine Turbopumps," see TSP's [page 1].*

Inquiries concerning rights for the commercial use of this invention should be addressed to the Patent Counsel, Marshall Space Flight Center [see page 1]. Refer to MFS-27304.

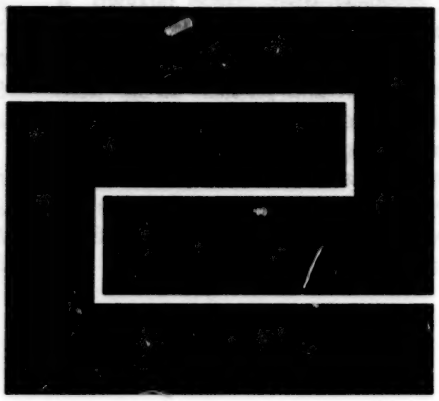

Fabrication Technology

Hardware, Techniques, and Processes

43 Screen-Cage Ion Plating of Silver on Polycrystalline Alumina

Screen-Cage Ion Plating of Silver on Polycrystalline Alumina

The silver adheres tenaciously and reduces friction.

Lewis Research Center, Cleveland, Ohio

A screen-cage ion-plating (SCIP) process applies silver films to complexly shaped substrates of polycrystalline alumina. The SCIP process is a modified version of an older direct ion-plating process that yields adherent coats on electrically conductive materials, but not on electrically nonconductive materials like alumina and other ceramics. The success of SCIP holds promise for applying lubricating soft metallic films to high-temperature ceramic components of advanced combustion engines to reduce friction and wear. Other potential uses for SCIP include coating substrates with metal for protection against corrosion, depositing electrical conductors on dielectric substrates, making optically reflective or electrically or thermally conductive surface layers, and applying decorative metal coats to ceramic trophies or sculptures.

The effectiveness of ion plating is attributed to its ability to provide a high-energy flux of ions and energetic neutral atoms that contribute to the adherence and desirable microstructure of the deposited film. An important additional advantage of this technique is known in the industry as "throwing power" — the ability to deposit a substantial amount of the anode material all over the substrate, including places that are not on direct lines of sight from the anode.

The older ion-plating process involves a diode configuration in which the substrate to be coated is connected as the cathode in a high-voltage dc circuit, while an evaporative source of material to be deposited is connected as the anode. Prior to deposition, the deposition chamber is evacuated, then backfilled with argon. Typical deposition conditions are: potential between –2 and –5 kV applied to the substrate, argon pressure between 10 and 20 mtorr (between 1.3 and 2.7 Pa), and current density between 0.2 and 0.5 mA/cm^2. Because the substrate must be conductive to act as the cathode, this process does not work for nonconductive substrates.

The present screen-cage version of the ion-plating process also involves a diode configuration, but in this case, the substrate (alumina or another electrically nonconductive material) is surrounded by a 20-mesh silver screen cage, to which the negative potential is applied. The cage functions as both an electronic grid and as part of a cathode. A combination of effects maintains zero electric field between the screen cage and the substrate: ions pass through the grid to the substrate, while secondary electrons emitted by the grid neutralize the positive charge that the incident ions contribute to the surface of the substrate. The gap between the screen cage and the surface of the substrate is critical and generally should be kept small (of the order of 6 mm). If the gap is too large, a hollow-cathode discharge occurs and causes excessive heating.

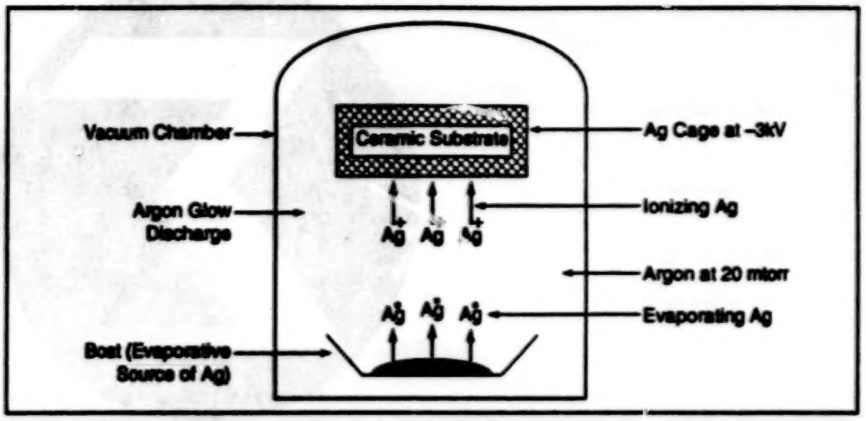

Figure 1. Screen-Cage Ion Plating is a cost-effective technique that offers high throwing power for deposition of adherent metal films on ceramic substrates.

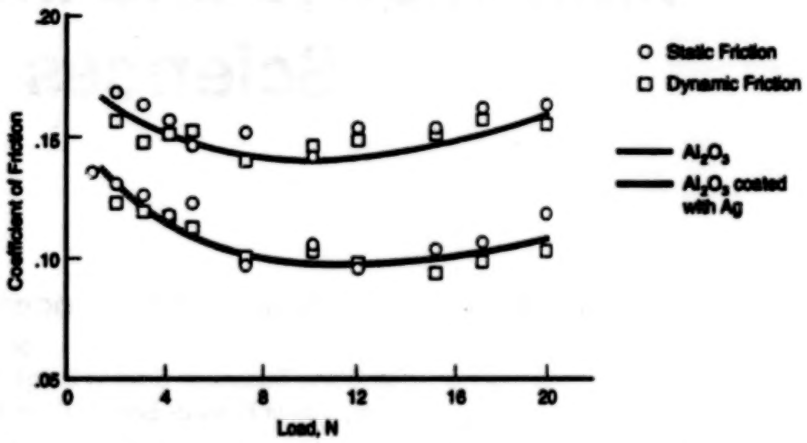

Figure 2. Coefficients of Friction of silver-coated and uncoated alumina surfaces were measured in constant-load scratch tests.

In one experiment to demonstrate the process, a film of silver 2 to 3 μm thick was deposited on an alumina substrate under the following conditions: effective cathode area 48 cm^2, potential of –3 kV applied to the screen cage, and current 80 mA. Because of the high throwing power, all exposed alumina surfaces were coated with silver. Even the surface facing away from the source was coated to a thickness about 1/3 that of the surface facing the source.

To assess the adherence and the lubricating ability of films deposited by this process, scratch tests and scratch-test measurements of friction were performed with a commercial scratch tester with a diamond stylus on both uncoated and silver-coated alumina surfaces. Subsequent analyses of the scratches by scanning electron microscopy and x-ray energy-dispersive spectrometry showed that significant amounts of silver remained, even where high stylus loads gave rise to severe crack patterns in the alumina. Coefficients of friction were lower on the alumina-coated surfaces, as shown in Figure 2.

This work was done by Talivaldis Spalvins, Harold E. Sliney, and Daniel L. Deadmore of **Lewis Research Center.** *Further information is contained in a TSP [see page 1].*

LEW-15858

Mathematics and Information Sciences

Hardware, Techniques, and Processes

45 Computer-Assisted Search of Large Textual Data Bases

46 Reducing Truncation Error in Integer Processing

46 Reduction of Sizes of Semi-Markov Reliability Models

Computer-Assisted Search of Large Textual Data Bases

Retrieved paragraphs are ranked according to measures based on semantics and relevance.

John F. Kennedy Space Center, Florida

"QA" denotes a high-speed computer system for searching diverse collections of documents including (but not limited to) technical reference manuals, legal documents, medical documents, news releases, and patents. QA incorporates both previously available and emerging information-retrieval technology to help a user intelligently and rapidly locate information found in large textual data bases. This technology includes (1) provision for inquiries in natural language; (2) statistical ranking of retrieved information; (3) an artificial-intelligence implementation of semantics, in which "surface level" knowledge found in text is used to improve the ranking of retrieved information; and (4) relevance feedback, in which the user's judgements of the relevance of some retrieved documents are used automatically to modify the search for further information.

A typical commercially available text-retrieval system uses a Boolean combination of key words supplied by the user to retrieve documents. In general, such a system does not rank the retrieved documents in any order of importance, so that the user needs to examine every retrieved document: this is a serious shortcoming when large collections of documents are searched. QA, however, does perform such a ranking.

The natural-language-inquiry and statistical-ranking features are not unique to QA but they are rare; they are available in only three commercial text-retrieval systems in the United States. The semantic and relevance-feedback features are not available in a commercial text-retrieval system and have been shown to yield a substantial improvement in the statistical ranking of retrieved information.

The semantic feature involves mathematical modeling on the basis of two concepts useful in talking informally about the real world: the concept of entities (objects in the real world) and the concept of relationships among entities (actions in the real world). Both entities and relationships have attributes. There are basic or surface-level attributes for entities in the real world. Examples of surface-level attributes of entities include size, color, and position.

Thematic-Role Categories	Attribute Categories
Accompaniment	Color
Amount	External and Internal Dimensions
Beneficiary	Form
Cause	Gender
Condition	General Dimensions
Comparison	Linear Dimensions
Conveyance	Motion Conjoined with Force
Degree	Motion in General
Destination	Motion with Reference to Direction
Duration	Order
Goal	Physical Properties
Instrument	Position
Location/Space	State
Manner	Temperature
Means	Use
Purpose	Variation
Range	
Result	
Source	
Time	

The 36 Semantic Categories are triggered by words in the semantic lexicon.

Words for these properties are prevalent in natural language. In linguistic research, the basic properties of relationships are called, variously, "thematic roles," "semantic roles," and "case roles." Thematic roles are prevalent in natural language; they reveal how sentence phrases and clauses are semantically related to the verbs in a sentence.

The primary goal of the QA System has been to detect thematic and attribute information (see table) contained in natural-language queries and documents. When such information is present, QA uses it to help find the paragraph most relevant to a query. The use of this information involves quantification of the relevance of the paragraph in terms of a similarity measure. Statistical weights used in computing the similarity measure are related to the frequency with which the words in the query trigger thematic roles and/or attributes as found in the Semantic Lexicon.

The relevance-feedback feature overcomes one of the deficiencies of commercial information-retrieval systems; namely that often, a system of this type retrieves only a few relevant documents if the search process is based solely on the initial query. This indicates a need to modify the query to improve performance; thus, it is customary to search the relevant documents iteratively in a sequence of partial searches. In other words, the results of earlier searches are used as feedback information to improve the results of later searches. In QA, this feedback concept is formalized and automated. QA asks the user to judge the relevance of some of the retrieved documents. The resulting data on relevance are used to formulate an improved query and recalculate the similarities between documents and the query in order to re-rank the documents.

This work was done by James R. Driscoll of the University of Central Florida for Kennedy Space Center. Further information is contained in a TSP [see page 1].

In accordance with Public Law 96-517, the contractor has elected to retain title to this invention. Inquiries concerning rights for its commercial use should be addressed to

James R. Driscoll
University of Central Florida
Computer Science
P.O. Box 162362
Orlando, FL 32816-0450

Refer to KSC-11707, volume and number of this NASA Tech Briefs *issue, and the page number.*

Reducing Truncation Error in Integer Processing

Signs of contributing errors are changed on alternate occurrences.

NASA's Jet Propulsion Laboratory, Pasadena, California

An improved method of rounding off (that is, truncation of least-significant bits) in integer processing of data has been devised. The method provides for the reduction, to an extremely low value, of the numerical bias that would otherwise be generated by accumulation of truncation errors from many arithmetic operations. The method was devised for use in integer signal processing, in which rescaling and truncation are usually performed to reduce the number of bits, which typically builds up in a sequence of operations. The essence of this method is to alternate the direction of roundoff (+, then −) on alternate occurrences of truncated values that contribute to the bias.

As an example, a 2's complement 5-bit integer is commonly reduced to a 3-bit integer by first adding the binary number 10 and truncating the last 2 bits. The possible errors in this truncation are −1/4, 0, and +1/2 relative to the retained integers. These truncation errors average to zero when a properly distributed population of integers is processed and combined, except for the error of −1/2. For example, errors of +1/4 and −1/4 cancel each other if the distribution of processed errors is symmetrical about zero, but errors of −1/2 cannot be combined with errors of +1/2 to average out to zero because there are no errors of +1/2 in this scheme. Instead, errors of −1/2 combine to contribute a bias of $-N_b/2$, where N_b is the number of occurrences of −1/2 in the processed population.

In the improved method, digital logic checks every input value to determine whether it can cause a truncation error of −1/2. Each time it encounters such a value, it changes the direction of roundoff to opposite the direction of roundoff on the most recent previous occurrence of such a value. Thus, errors of −1/2 become −1/2, +1/2, −1/2, and so forth. This forces the overall bias to be either 0 or −1/2, depending on whether the string contains an even or odd number of −1/2's. Thus, this method reduces the cumulative truncation error from $N_b/2$ to 0 or 1/2. Since N_b can be a very large number, this reduction can be enormous. Further, when it is known that N_b is odd, the bias of 1/2 will be known and can be removed.

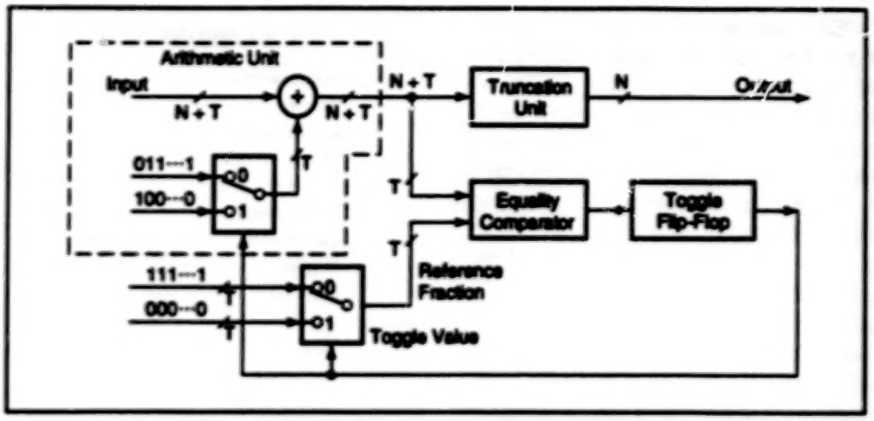

A Truncation Circuit that implements the improved method includes a comparator that determines whether the fractional part, *T* bits, of the incoming number equals 100···0. If it does, the toggle flip-flop resets the toggle value to the alternate position.

In one of several possible implementations of the method (see figure), the current toggle value determines whether an increment of 011···1 or 100···0 is to be added to the current incoming integer which has *N* most significant bits and *T* least significant bits (LSBs). After the addition, the fractional part, the *T* LSBs, is compared with either 111···1 or 000···0, again according to the current toggle value to determine whether the incoming fractional part had been 100···0. If it was, the toggle is flipped and the alternate increment is applied to all subsequent integers until the next time that the LSBs are equal to 100···0. With this scheme, the −1/2's are alternately rounded up and down, while all other fractional values are rounded in the conventional manner.

This work was done by J. Brooks Thomas, Jeffrey B. Berner, and J. Scott Graham of **NASA's Jet Propulsion Laboratory.** *Further information is contained in a TSP [see page 1].*

NPO-18968

Reduction of Sizes of Semi-Markov Reliability Models

A trimming technique reduces computational effort by an order of magnitude while introducing negligible error.

Langley Research Center, Hampton, Virginia

Semi-Markov processes have proved to be both effective and convenient for constructing mathematical models of systems that are made reliable by use of redundancy and the capability of reconfiguration. These models can depict complicated systems and capture (via simulation) the essential features of the dynamics of the arrival of faults and the recovery of systems from faults. One disadvantage is that the models can be extremely large, posing problems both of construction and of computation. Sound and effective procedures to reduce the sizes of the models ("model-reduction methods" for short) are needed.

Because the systems represented by the models are used in critical applications, an acceptable model-reduction method must provide for an analytically derived error bound. A model-reduction method must be easy to implement, and the error bound easy to compute. A model-reduction method called "trimming" can be applied to a popular class of systems, and an error bound for this method depends on readily available parameters of the modeled system.

The error bound depends on only three parameters from the semi-Markov model: the maximum sum of rates for failure transitions leaving any state, the maximum average holding time for a recov-

ery-mode state, and the operating time for the system. The error bound can be computed before any model is generated, enabling the modeler to decide immediately whether or not the model can be trimmed. The trimming procedure is specified by a precise and easy description, which makes it easy to include the trimming procedure in a program that generates mathematical models for use in assessing reliability.

Two models, complete and trimmed, were constructed for a sample system by use of the ASSIST reliability-model-generating computer program. The complete model contained 227 states and took 7,878 seconds to compute. The trimmed model contained 83 states and took 258 seconds to compute. The relative error produced by model trimming was approximately 1 part in 10 million, while the error bound for model trimming was approximately 1 part in a thousand. The results from this example are typical for an application of trimming. The number of states in the reliability model was reduced by about half. The computational effort was reduced by an order of magnitude. The actual error from trimming was insignificant. The derived error bound for trimming was much larger than the actual error, but still small in comparison with the computed probability of failure of the system.

A typical application of this technique is in the design of digital control systems that are required to be extremely reliable. An example is the proposed requirement that the probability of failure of the flight-control system of a commercial aircraft during a 10-hour flight be less than 1 billionth. In addition to aerospace applications, fault-tolerant design has growing importance in a wide range of industrial applications. Simple, intuitive analytic methods like this one should help strengthen industrial practice.

This work was done by Allan L. White and Dan L. Palumbo of **Langley Research Center** *Further information may be found in NASA TP-3089 [N91-25741], "Model Reduction by Trimming for a Class of Semi-Markov Reliability Models and the Corresponding Error Bound."*

Copies may be purchased [prepayment required] from the NASA Center for AeroSpace Information, Linthicum Heights, Maryland, Telephone No. (301) 621-0390. Rush orders may be placed for an extra fee by calling (800) 336-4700.
LAR-14363

Life Sciences

Hardware, Techniques, and Processes

49 Finger-Circumference-Measuring Device

Finger-Circumference-Measuring Device

An easy-to-use device provides data on volumetric changes.

Lyndon B. Johnson Space Center, Houston, Texas

An easy-to-use device quickly measures the circumference of a finger (including the thumb) on a human hand. The device was designed to facilitate measurements at various points along the fingers to obtain data for studies of volumetric changes of the fingers in microgravity. It could also be used in normal Earth gravity; for example, in studies of growth and in assessment of diseases like arthritis.

The device includes a polytetrafluoroethylene band 1/8 in. (about 3 mm) wide, bent into a loop and attached to a tab that slides on a scale graduated in millimeters (see figure). The sliding tab is preloaded with a constant-force tension spring, which pulls the tab toward closure of the loop. Holding the device with either hand, the user pushes the sliding tab to expand against the spring force to expand the loop, then slips the band over a finger and holds it at a point of interest such as a joint or the midlength position along a phalange. The user then releases the sliding tab, allowing the spring to pull the band snugly around the finger. The position of the sliding tab on the scale indicates the circumference of the finger in millimeters.

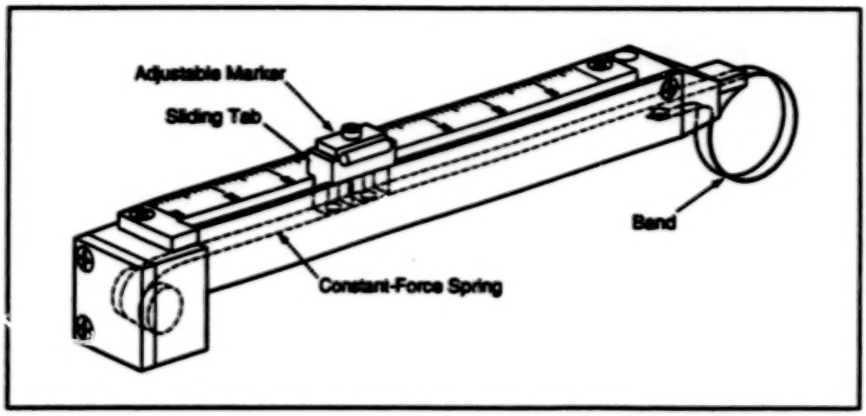

This Device Measures Circumference of a finger or other round object placed in the loop. Measurements are accurate to within ±1 mm in a range of 25 to 100 mm.

The spring is made of stainless steel and exerts a constant force of 3 oz (about 0.8 N) on the band. The spring is wound on a polytetrafluoroethylene spool at the end of the scale opposite the band. The sliding tab is made of Delrin™ acetal polymer. The materials of each part were selected for resistance to wear, low friction, nonflammability, flexibility, and/or elasticity, as applicable. The device weighs only 4 oz (has a mass of about 110 grams).

For calibration, the band is tightened around a rod machined to a known diameter or circumference. The marker on the sliding tab is then adjusted to obtain the correct reading.

This work was done by Suy Le of **Johnson Space Center**. *Further information is contained in a TSP [see page 1].*
MSC-22332

National Aeronautics and
Space Administration

50

END

DATE FILMED

08/24/95